

We are IntechOpen, the world's leading publisher of Open Access books Built by scientists, for scientists

6,900

Open access books available

186,000

International authors and editors

200M

Downloads

Our authors are among the

154

Countries delivered to

TOP 1%

most cited scientists

12.2%

Contributors from top 500 universities



WEB OF SCIENCE™

Selection of our books indexed in the Book Citation Index
in Web of Science™ Core Collection (BKCI)

Interested in publishing with us?
Contact book.department@intechopen.com

Numbers displayed above are based on latest data collected.
For more information visit www.intechopen.com



Pico- and Femtosecond Laser Micromachining for Surface Texturing

Tatsuhiko Aizawa and Tadahiko Inohara

Abstract

The pico- and femtosecond laser micromachining has grown up as a reliable tool for precise manufacturing and electronic industries to make fine drilling and machining into hard metals and ceramics as well as soft plastic and to form various nano- and microtextures for improvement of surface functions and properties in products. The ultrashort-pulse laser machining systems were developed to describe the fine microdrilling and microtexturing behavior for various materials. Accuracy in circularity and drilled depth were evaluated to discuss the effect of substrate materials on the laser microdrilling. Accuracy in unit geometry and alignment was also discussed for applications. A carbon base mold substrate was micromachined to transcribe its microtextures to transparent plastics and oxide glasses. Three practical examples were introduced to demonstrate the effectiveness of nano-/microtexturing on the improvement of microjoinability, the reduction in friction and wear of mechanical parts and tools, and the surface property control. The fast-rate laser machinability, the spatial resolution in laser microtexturing as well as the laser micromanufacturing capacity were discussed to aim at the future innovations in manufacturing toward the sustainable society.

Keywords: picosecond laser micromachining, femtosecond laser micromachining, microdrilling, microtexturing, nano-/microtexturing, laser micropatterning

1. Introduction

The laser technology for manufacturing is classified into two categories; e.g., thermal and athermal processings [1]. CO₂-laser with continuous power supply and fiber-lasers with use of short pulses are typical processing for welding, machining, and joining by formation of thermally hot spots [2]. Various fiber lasers [3] have been developed and applied to laser welding, laser machining, laser marking, and so on [3]. Most of them utilize the nanosecond solid-state oscillators and make thermal machining of materials. In recent, pico- and femtosecond laser machining [4–6] is widely utilized for athermal removal of materials with high dimensional accuracy in practice.

There are two keywords to classify the laser processing; i.e., the wave length of light and the pulse duration time. CO₂ laser has the longest wave length of 10.6 μm, while excimer laser by KrF, 248 nm. Most of laser wave length (λ) ranges from the far ultra-violet regime less than 200 nm to infra-red regime more than 20 μm. Since every material has its own relaxation time (τ_0), most of laser power can be absorbed by the material having the equivalent τ_0 to λ . Then, this targeting work material is athermally

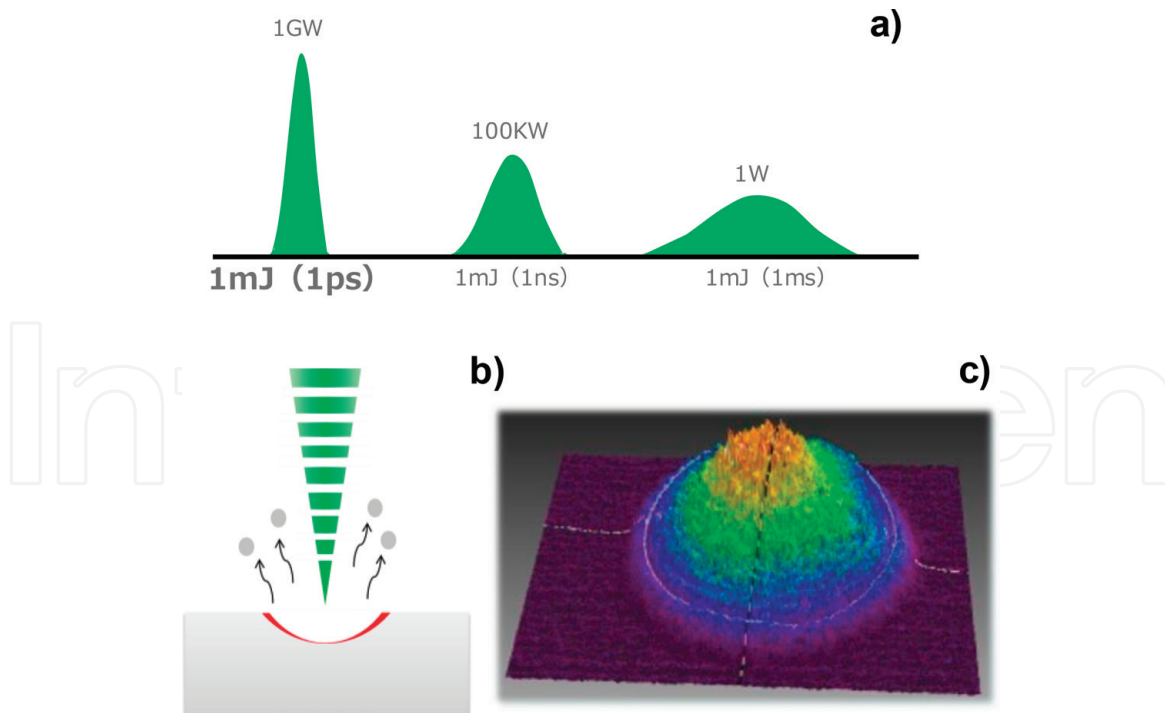


Figure 1. Typical characteristics of ultra-short pulse laser machining. (a) Significant increase of laser power by reduction of Δt down to 1 ps, (b) ablation as an athermal removal of materials, and (c) laser intensity profile.

machined by selecting the laser with suitable wave length; otherwise, the work is only thermally cut or drilled. A micromachining essentially requires for fast-rate removal of materials with sufficient accuracy in dimension and geometry; the repetition frequency as well as the wave length must be optimally selected to make suitable laser micromachining to each work-material. With use of second harmonic generator (SHG), third harmonic generator (THG), and fourth harmonic generator (FHG), the fundamental wavelength of 1064 nm is controllable to be 532, 355 and 266 nm, respectively.

The pulse duration time (Δt) is important for short-pulse laser micromachining. As shown in **Figure 1a**, the pulse power increases significantly with reduction of Δt . When the laser energy with $\Delta t = 1$ ms is 1 mJ, the laser power (P) is only 1 W; P reaches to 1 GW only by shortening Δt down to 1 ps.

Under high power laser irradiation, most of materials are athermally removed, or, ablated, as depicted in **Figure 1b**. The dimensional accuracy in laser micromachining is determined by focusing the laser spot for this ablation process. This laser irradiation has a finite spot size which is dependent on λ and Δt . The laser intensity distributes even in the focused spot; e.g., the well-controlled laser intensity distributes in Gaussian profile as depicted in **Figure 1c**.

In the following, our developing ultrashort pulse laser machining systems are employed to make microdrilling and microtexturing into various kinds of work materials. In particular, the laser microtexturing technology is applied to microjoining process of dissimilar polymers, and to microdimple formation for friction control of sliding parts and components and for reservoir of wear debris during dry cutting. Further applications including the surface property control by using the nano-/microtexturing are discussed in this chapter.

2. Pico- and femtosecond laser micromachining system

Our developed pico- and femtosecond laser machining systems are stated with some comments on their capacity and configuration.

2.1 Picosecond laser micromachining system

A single picosecond is equivalent to the relaxation time of molecular bonding stage; its pulsed power is readily absorbed by most of work materials. Three types of picosecond laser machining systems were developed; a standard system and its configuration are shown in **Figure 2**. The machining speed is dependent on the repetition frequency and average power. The dimensional accuracy in machining is determined by the beam spot size. To be discussed later, this spot size depends on the optical system; e.g., the minimum spot size can be controlled down to 1 μm when every lens is fixed on the stage. However, when the lens position is controlled during machining, the spot size becomes wider; e.g., it is limited by 10 μm when using the galvanometer.

2.2 Femtosecond laser micromachining system

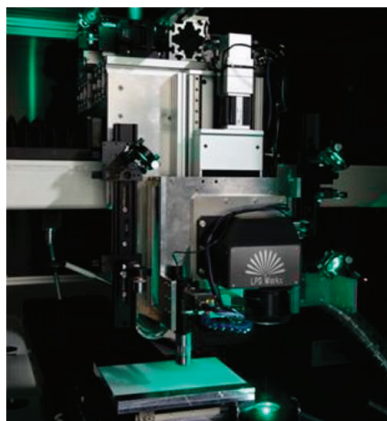
A single femtosecond or subpicosecond lasers are developed for innovative research and development; most industrial applications stand on this laser machining in the order of 100 femtoseconds. Our developed system and its configuration are shown in **Figure 3**.

Since the focused spot of work materials is subjected to ultra-high power irradiation, how to scan the beam spot becomes more important when using this laser machining system. Higher repetition frequency of laser beams as well as higher scanning speed result in fast-rate dimensionally accurate machining. At present, a laser oscillator with the repetition frequency of 40 MHz has been already developed for machining. How to make fast control of this short pulse laser becomes an essential issue in laser machining design.



Wave length	515nm
Pulse duration	<10ps
Average power	30W
Repetition	MAX200kHz
Beam spot size	MINΦ10μm using Galvanometer MINΦ1μm using fixed lens
Stage area	400mm\times400mm
Sample Weight	< 10kg

Figure 2.
 Our developed picosecond laser machining system and its capacity and configuration.



Wave length	515nm
Pulse duration	180fs~190fs
Average power	8.2W
Repetition	MAX600kHz
Beam spot size	MIN:10μm using Galvanometer MIN:1μm using fixed lens
Stage area	300mm\times300mm
Scanning speed	MAX 3000mm/s
Scanning area	MAX 30mm\times30mm
Sample weight	< 30kg

Figure 3.
 Our developed femtosecond laser machining system and its capacity and configuration.

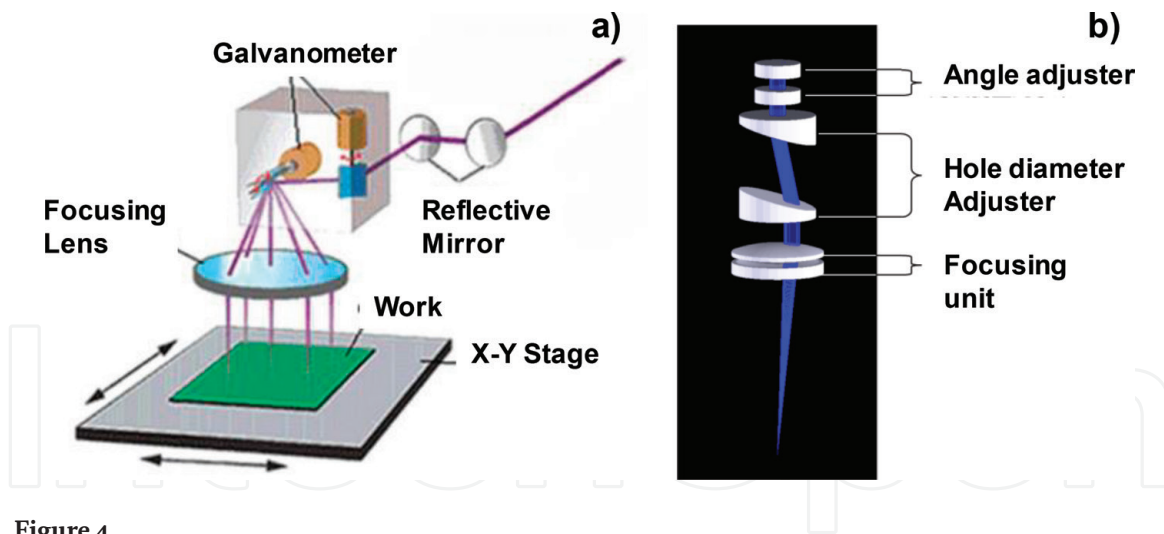


Figure 4. Typical two optical control units for laser micromachining. (a) Optical control unit with use of galvanometer and (b) beam rotator.

2.3 Optical unit control

In parallel with the development of laser oscillators and machining unit, the optical unit design is also important for accurate laser machining. Two unit designs are introduced in **Figure 4**; e.g., an optical control unit with use of galvanometer to distribute the laser beam as designed, and a beam rotator for laser drilling with accurate circularity. The former unit is a standard approach for laser machining with moderate rate; new controller must be developed to make much faster rate laser machining. The latter is a powerful tool to rotate the optical units and to move the laser beam in the axisymmetric manner.

Various controlling tools of laser beam can be designed and developed for each application of laser machining.

3. Fine microdrilling into metallic alloys and ceramics

These pico- and femtoseconds with the pulse duration in the order of 10^{-12} and 10^{-15} s provide a reliable means to drill the through-holes into the ceramics, the metallic alloys, and the plastics [7]. Compared to the micromilling and the microelectrical discharge machining (micro-EDM), finer through-holes with higher circularity are formed without residuals at the inlet of holes and without deterioration on their inner surfaces [8]. In addition, no micromilling tools and no thin EDM wires are needed to drill the lots of through-holes onto the relatively large area. In this laser drilling process, the surface quality of through-holes as well as their circularity is strongly dependent on the laser beam control, as summarized in [9]. In the conventional fiber-laser machining, the inlet of through-holes is deteriorated by the redeposits and the residuals [10]. Even when using the picosecond pulse lasers, the through-hole shape is also damaged by the unstable laser beams [11, 12]. Typical damage of through-holes comes from the branching from the straight hole drilled in the initial stage to two holes. The deviation of beam focusing and positioning directly induces these defects [7, 8, 13]. Our developed picosecond laser machining system for industrial applications is applied to drill the through-holes into the ceramic plates. The beam rotator is used as a trepanning system for laser drilling. The alumina plate with the thickness of 1 mm is employed as a substrate. Scanning electron microscopy (SEM) is used to measure the diameter of through-holes as well as their aspect ratio. The replica method is also utilized to describe the

geometric alignment and homogeneity of through-holes. The drilled through-holes with the uniform diameter of 50 μm and the aspect ratio of 10.0 are accurately aligned into the alumina plate. The present trepanning device works to control the diameter of irradiation for fine drilling of the tapered and inversely tapered through-holes into steels.

3.1 Microdrilling into ceramic substrates

The alumina plate is prepared for the laser drilling under the experimental setup in **Figure 5**. The beam rotator as well as projection lens unit is utilized to improve the focused beam quality. Through the CCD and display, the microdrilling process is monitored during operation.

Let us first evaluate on the difference of drilling behavior between the fiber lasers and the picosecond laser. The through-hole with the diameter of 50 μm is drilled into alumina plate. When using the normal fiber lasers, the surroundings of hole are completely damaged with deposits on them **Figure 6a**. While, the accurate hole with circularity of 1 μm is drilled by the picosecond laser without damage and deposits, as shown in **Figure 6b**.

No residuals or no redeposits at the vicinity of through-hole inlets prove that the present picosecond laser drilling is free from the thermal effects to deteriorate the surface quality of work specimen. The picosecond laser drilling is utilized to

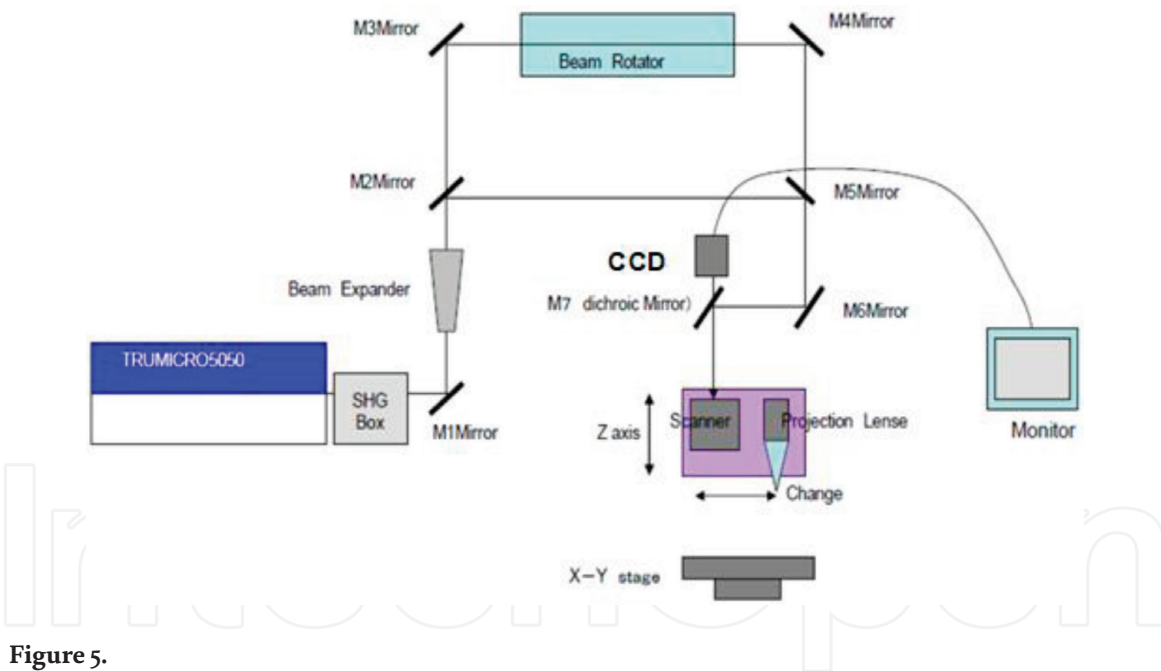


Figure 5.
A typical experimental setup for laser microdrilling.

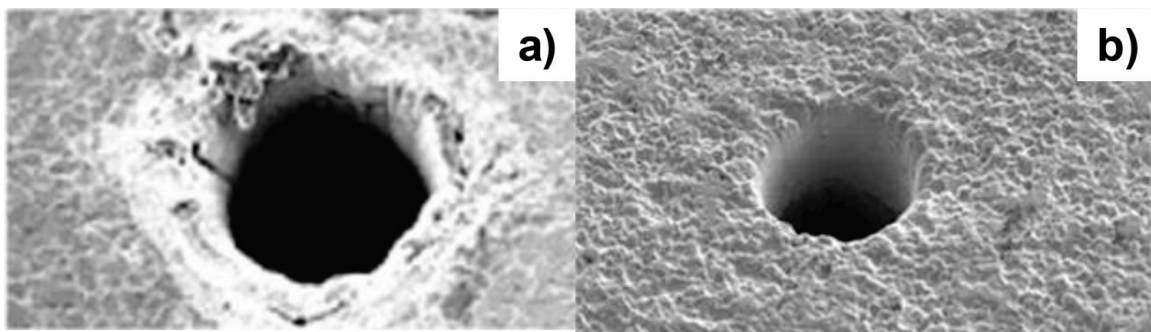


Figure 6.
Comparison of the drilled through-hole between fiber lasers and the picosecond laser. (a) Fiber laser drilling, and, (b) Picosecond laser drilling.

fabricate a series of holes with periodically aligned into alumina substrate. **Figure 7a** depicts the through-holes drilled into the alumina. Each through-hole is aligned with the pitch of $300\ \mu\text{m}$ as programmed by the CAM data mining through the positioning control of beams. As had been discussed in [11], the inner surface quality of through-holes is sensitive to the instability during the laser drilling. **Figure 7b** also demonstrates that the straight through-hole inner surfaces are formed to have constant diameter without any geometric damages by the picosecond laser drilling. This is because the laser beam is well profiled through the trepanning system before fine control by the galvanometer, and is controlled to move into the depth of work materials. The above straightforwardness of through-holes is also demonstrated by using the replica method. In this method, the silicone-based polymers are infiltrated into each through-hole. The frozen polymers are used as a replica to reproduce the drilled through-hole shape. **Figure 7c** depicts the alignment of replicas in correspondence to a series of laser-drilled through-holes. Three through-holes were laser-drilled down to the same depth in the alumina plate. Since the first three polymer pillars have the same height as $150\ \mu\text{m}$, the successive series of through-holes are accurately machined into the alumina with the same depth.

These straight through-holes with high aspect ratio provide a solution to the demand for the probe-cards to make accurate inspection of the semiconductor

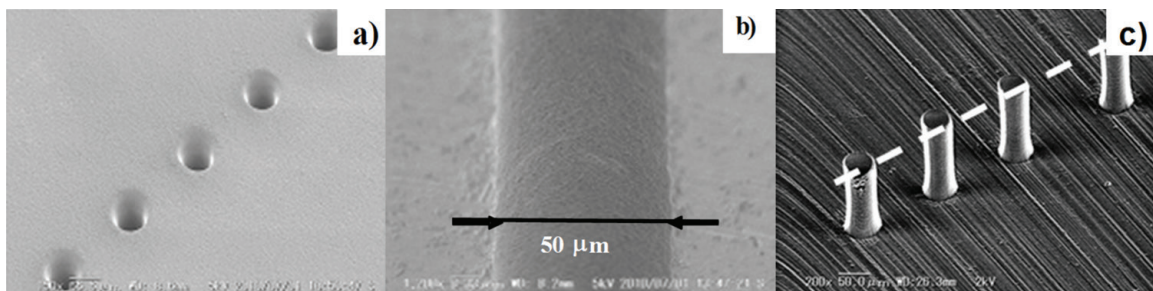


Figure 7. Pico-second laser drilling of through-holes into the alumina plate. (a) Alignment of through-holes, (b) inner surface of through-hole with the diameter of $50\ \mu\text{m}$, and (c) demonstration of the homogeneous laser drilling by using the replica method.

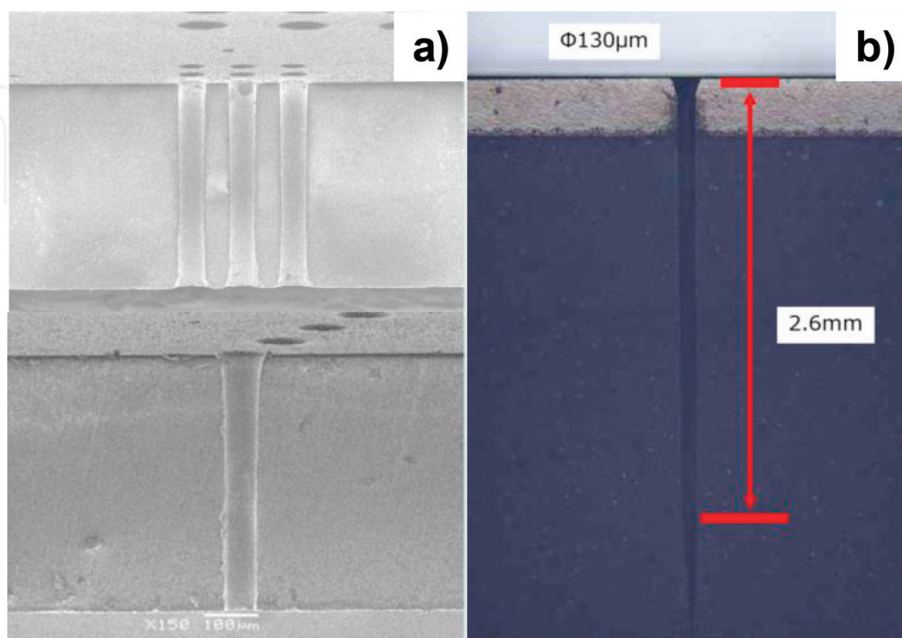


Figure 8. Pico-second laser drilling of through-holes with higher aspect ratio. (a) Drilled through-holes into alumina plate and (b) drilled through-holes into partially stabilized zirconia (PSZ).

chips. The probe-pins are pierced through the straight through-holes of alumina or PSZ substrates for inspection. These through-holes must have higher aspect ratio than 10 to preserve the sufficient working space. **Figure 8a** depicts the through-hole with the diameter of 50 μm machined into the alumina plate with the thickness of 1 mm; the aspect ratio reaches to 20. This high aspect ratio is also attained even when laser drilling PSZ in **Figure 8b**. This demonstrates that the trepanned laser drilling enables to make through-holes with higher aspect ratio than 20 under the well-structured setup in laser machining.

3.2 Microdrilling into metallic alloys

In the die and mold industries, the case-hardened and plasma-treated steels are often utilized for high proof of dimensional accuracy. Let us also compare the laser drilling performance between the fiber-lasers and the picosecond laser. **Figure 9** compared the drilled through-holes between two lasers. The large heat-affected zones as well as damages surround the drilled hole by fiber laser in **Figure 9a**. While, the clean and accurate through-hole is drilled into the case-hardened steels by the picosecond laser in **Figure 9b**.

Without use of the beam rotation control, the tapering is difficult or nearly impossible in the laser drilling. In the present setup, the pair of lenses in the beam rotator in **Figure 5** is radially adjusted to directly control the diameter of irradiated

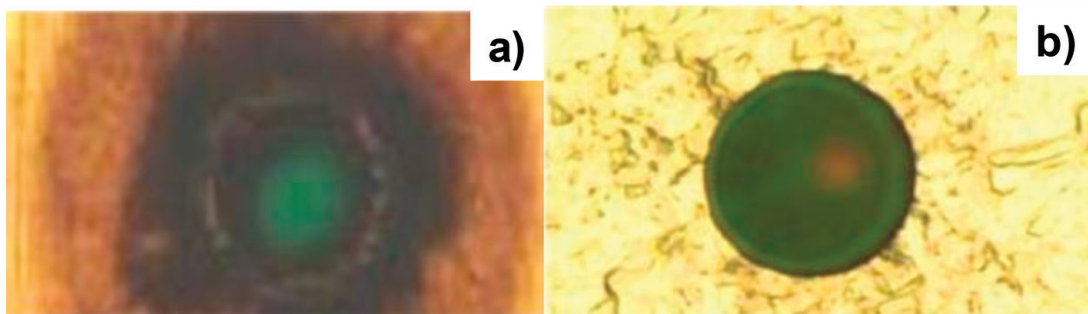


Figure 9. Comparison of the drilled through-holes into the case-hardened steels. (a) Using the fiber lasers and (b) using the picosecond laser.

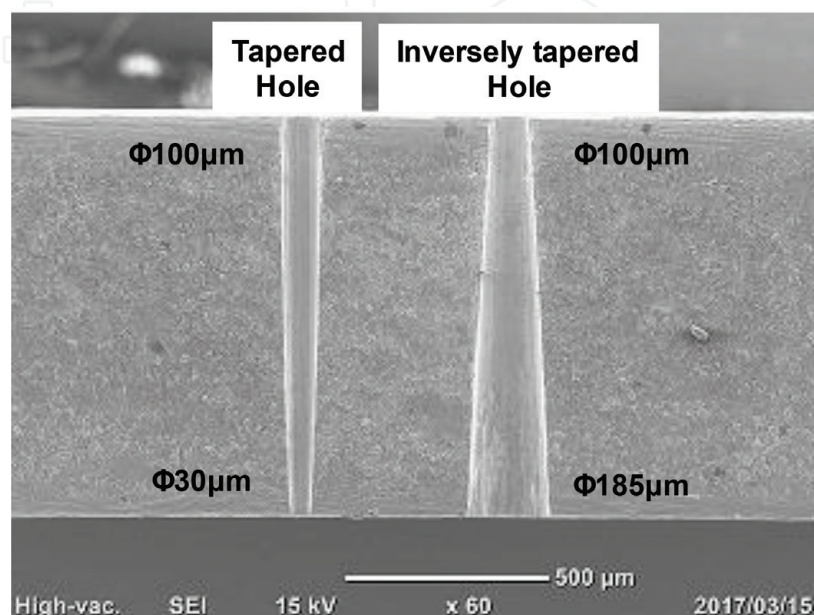


Figure 10. Picosecond laser drilling of the tapered and inversely tapered through-holes into the case-hardened steels.

region. When this diameter is narrowed from the inlet to the outlet with the constant velocity, the uniformly tapered through-hole is drilled to have a constant tapered angle up to the specified positive skew angle. On the other hand, the inversely tapered through-hole is also machined by enlarging this diameter with the constant velocity in the similar way down to the negative skew angle. These tapering or inversely tapering processes from the inlet to outlet of the through-hole are automatically programmed. After CAM data in the present laser drilling, this diameter of irradiation is narrowed from the inlet by $100\ \mu\text{m}$ to the outlet by $30\ \mu\text{m}$ with the constant feeding velocity. Then, the tapered through-hole is built into the alumina plate with the constant angle of $+30^\circ$ and the higher aspect ratio than 10.0 in **Figure 10**. In the similar way, the inversely tapered through-hole is formed by enlarging the diameter of irradiation from the inlet by $100\ \mu\text{m}$ to the outlet by $180\ \mu\text{m}$ also with the constant velocity. The inversely tapered through-hole is also drilled into the alumina with the thickness of 1 mm. The inversely tapered angles are also constant by -25° . In both cases, the inner surfaces of holes are finely shaped with less roughness [14].

4. Fine microtexturing onto metallic alloys and polymers

Microtextures with the size in the order of $1\text{--}100\ \mu\text{m}$ on the solid surface and interface work to reduce the friction and wear, to assist the joinability, and to functionalize the surfaces and interfaces [15]. Micromilling [16] and microelectrical discharge machining (micro-EDM) [17] have been utilized to make microtexturing onto the steel surfaces. Due to the limitation on the machining tool shape and their controllability for machining, their application is also limited in practice. Short-pulse laser machining is employed to make microtexturing onto the metallic and ceramic surfaces.

4.1 Microtexturing of dimples onto the surfaces

A circular dimple is formed on the various metallic surfaces as an aligned structure. **Figure 11** depicts four microtexturing cases. The unit-geometry of microdimples, their alignment on the surfaces, and the finished surface quality are preserved with less roughing during laser processing. For an example, the circular microdimples with the diameter of $95\ \mu\text{m}$ and the depth of $26\ \mu\text{m}$ are formed on the AISI430 surface in the pitch of $110\ \mu\text{m}$ as shown in **Figure 11d**. No difference

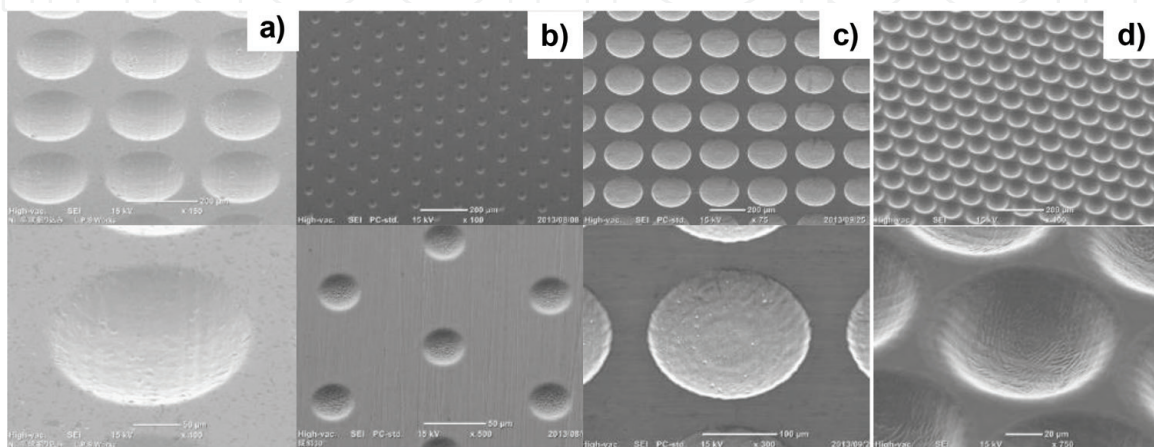


Figure 11. Laser microtexturing of circular dimples aligned on the metallic substrates. (a) Aluminum, (b) copper, (c) nickel, and (d) AISI430.

in microdimple size and shape and in its alignment is noticed for various kinds of metallic substrates.

4.2 Microtexturing of embosses onto the surfaces

The initial geometric data in CAD and CAM for laser microdimple texturing are data-transformed from positive to negative; this transformed CAD and CAM data are automatically built for laser microemboss formation. In practice, the concave patterning to form the microdimples changes itself to the convex patterning to form the microembosses onto the substrate surfaces. **Figure 12** depicts four microembossing cases. The dimensional and geometric accuracies are preserved in the similar manner of microdimple formation. For an example, the circular microembosses with the diameter of 250 μm and the depth of 125 μm are formed on the boron-silicate glass surface in the pitch of 280 μm , as shown in **Figure 12d**.

4.3 Microtexturing of 3D-lattice structures onto the surfaces

With use of femtosecond lasers, finer microtextures are formed as a three-dimensional structure on the metallic surfaces. **Figure 13** depicts the three-dimensional microstructures formed on the steel surfaces. In particular, the

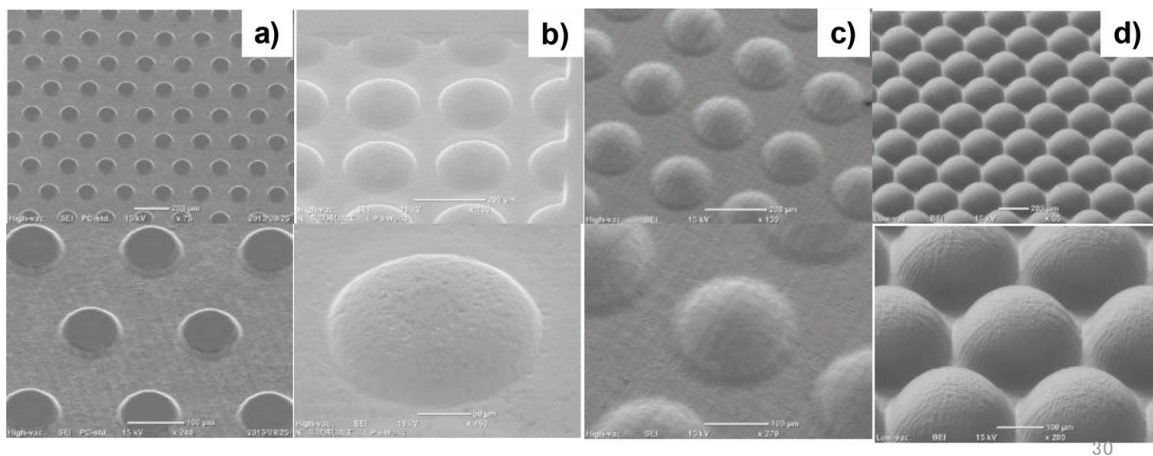


Figure 12. Laser microembossing of circular embosses aligned on the metallic and ceramic substrates. (a) AISI430, (b) Ni, (c) AISI304, and (d) boron-silicate glass.

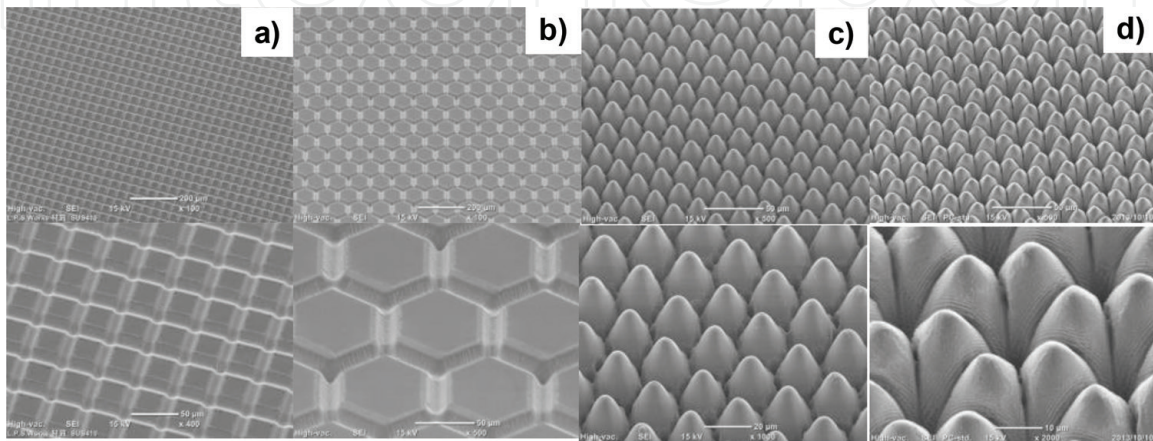


Figure 13. Laser microtexturing of three-dimensional structures onto the surfaces. (a) AISI410, (b) SISI304, (c) AISI430, and (d) AISI430.

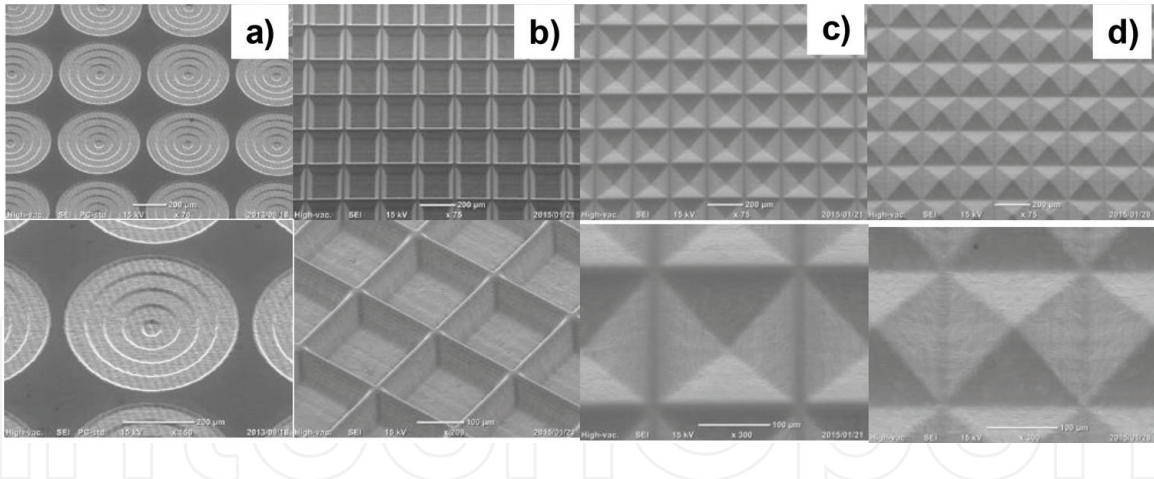


Figure 14. Laser microtexturing of fine periodic structures onto the surfaces. (a) Al, (b) AISI304, (c) AISI304, and (d) AISI304.

Gaussian-shaped pillar array with the height of 20 μm and the pitch of 20 μm is machined into the AISI430 substrate as shown in **Figure 13c**.

4.4 Microtexturing of periodic structures onto the surfaces

Three-dimensional periodic microstructures have a capability to functionalize the metallic surfaces for optical reflection and diffraction devices and for stamping die and injection mold to transcribe their negative textures onto metallic and polymer sheets. **Figure 14** depicts the periodic microstructures formed on the aluminum and AISI304 steel substrates, respectively. **Figure 14a** is a stepwise terrace structure machined into aluminum with each layer thickness of 5 μm by decreasing the diameter from 450 μm down to 50 μm with the step of 100 μm .

5. Fine microtexturing into carbon-base molds

Two- and three-dimensional microtexturing becomes much important in preparation of mold-dies for mold-stamping of optical elements [18]. The most popular microtexture is a Fresnel pattern for optical lens; circumferential patterns with steep surfaces must be imprinted onto the surface of substrate materials. V-letter-shaped micropatterns are laser-machined onto the glassy carbon substrate to discuss the dimensional accuracy and to investigate the depth profile for different aspect ratio. Furthermore, our developing microstamping system [8, 19, 20] is utilized to duplicate these micropatterns onto optical polymers by using the patterned glassy carbon mold-dies and to discuss the accuracy by this imprinting.

5.1 Microtexturing into glassy carbon die substrate

In the two-dimensional microtexturing, a unit pattern like a groove, a dimple, or a wedge is machined with the specified regularity onto the substrate by using X-Y positioning control. Here, a microgroove is employed as a standard unit pattern to fabricate the microtextured mold-die. Glassy carbon (GC) substrate is employed to make V-letter-shaped microgrooving with the pitch of 35 μm , the V-shaped wedge width of 10 μm , and the depth of 10 μm in design. **Figure 15a** shows the optical micrograph of V-shaped grooving pattern on GC substrate. One groove is laser-machined twice on the same designed machining path. This micropattern is formed onto the GC substrate with the area of 25 \times 25 mm² for 40 min or 2.4 ks. As shown in **Figure 15b**, a sharp

wedge of microgroove is imprinted onto the multilayered GC substrate. The microgroove has 10 μm in width, and 35 μm in pitch. The geometric dimensions specified in CAM program are accurately reproduced in the actual laser microtexturing. The depth profile of V-letter-shaped microgrooves is directly measured to investigate the accuracy of depth in the two-dimensional texturing. **Figure 16** depicts the measured depth profile by precise surface profilometer. Deviation of depth ranges from -1 to $+2$ μm around the average depth of 10 μm . This proves that regular patterns could be machined by the present approach. In order to investigate the controllability of microgrooving in depth, the designed depth parameter is varied with the laser beam power kept constant. **Figure 17** compares the relationship between the designed and

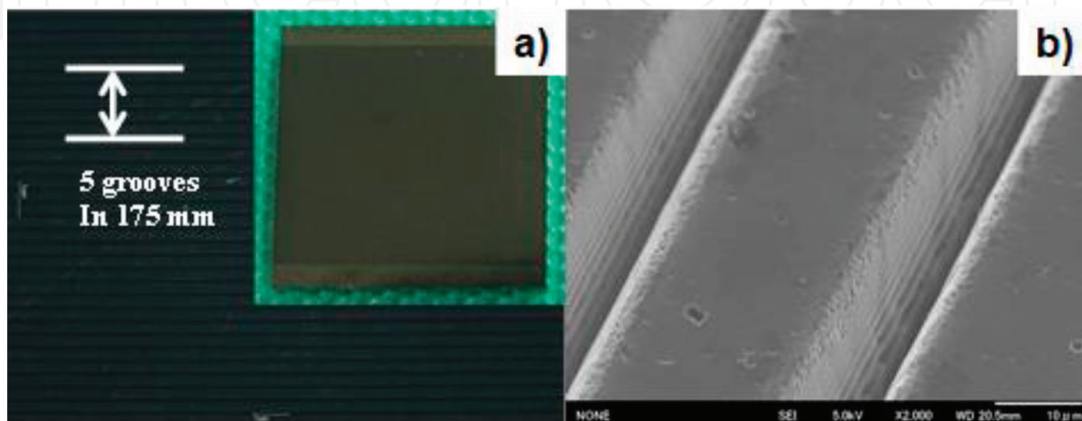


Figure 15.
Laser microtexturing of V-letter shaped grooves into GC substrate. (a) Microscopic image of microgrooved GC and (b) SEM image of microgrooves.

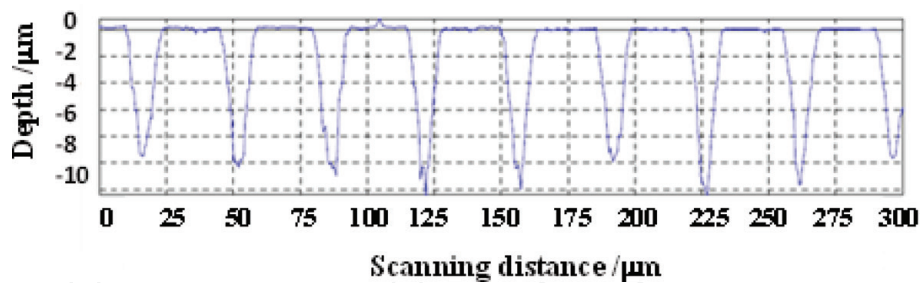


Figure 16.
Depth profile across the V-letter shaped microgrooves in GC substrate.

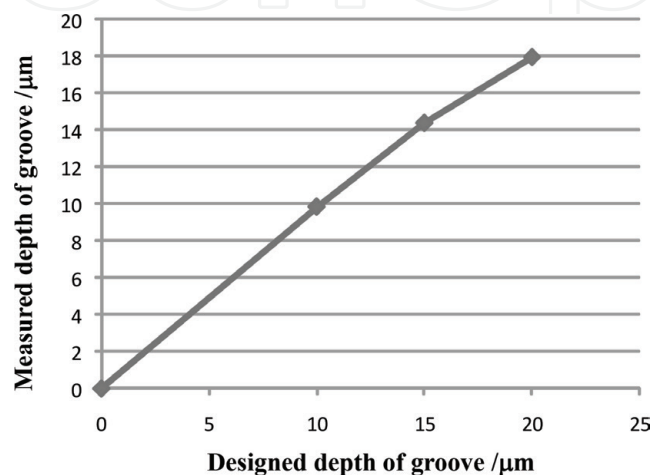


Figure 17.
Relationship between the designed and measured microgroove depths.

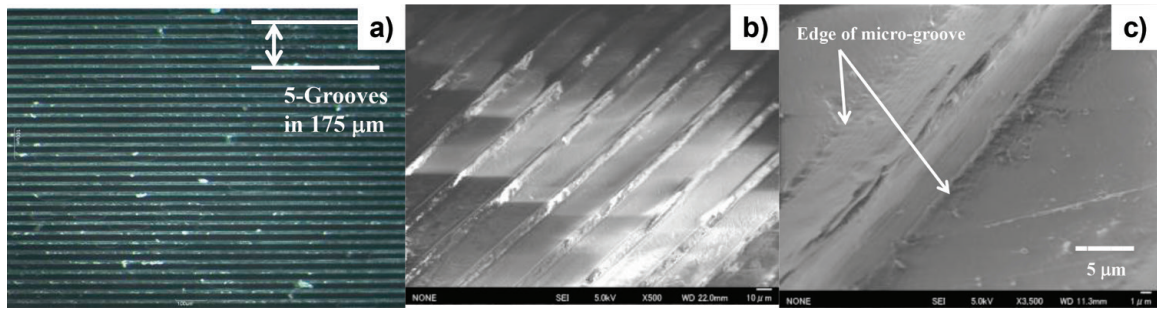


Figure 18.

Transcription of the V-letter wedge microtexture on GC to the V-letter bump microtexture via the mold stamping. (a) Multimicrogrooved PMMA sheet, (b) V-letter bump microtextures on PMMA, and (c) formation of microbump by inclusion of melt PMMA into V-letter wedge on GC mold.

measured depths in this microgrooving. Up to 20 μm , the average depth of microgrooves is accurately controlled by the present laser machining system.

5.2 Mold stamping into optical plastics

The above microtextured GC substrate is used as a mold-die for warm mold-stamping. PMMA sheet with the thickness of 1 mm is employed as a work material for this mold-stamping just above its glass-transition temperature of 383 K (or 110°C). **Figure 18a** showed the V-letter-shaped grooving patterns, which are imprinted onto PMMA by the load of 1 kN for 60 s. The V-letter-shaped concave patterns in **Figure 15b** are accurately imprinted onto PMMA as the convex micropattern as shown in **Figure 18b**. That is, a series of microwedge fins are fabricated by this mold-stamping with use of microtextured mold in **Figure 15**. In the mold-stamping, the filling process of work materials into the micropatterns on the mold-die is essential for accurate imprinting. Precise observation with higher magnification in SEM is made to investigate this filling behavior at the initial stage of mold-stamping. **Figure 18c** depicted a convex bump with the width of 10 μm and the height of 3.5 μm . This bump formation is just the initial stage of filling process for viscous PMMA to infiltrate into the V-letter-shaped groove by mold-stamping. In case of mold-stamping just above the glass transition temperature, viscosity of plastic materials is so high as to reduce the filling velocity. This reflects on the slow shearing along the side faces of microgroove.

6. Microjoining of dissimilar polymers by laser microtexturing

Most of mobile cellular phones are not water-proven so as to be diminished in the accident where those were dropped into water. To be free from these damages, there have been done many efforts to install the perfect waterproof into them [21]; e.g., a silicone rubber ring was sandwiched between plastic cover cases to prevent from water penetration through clearance. This fixture might work well just after shipping; it could be useless at the presence of dirt on the interface or through its misalignment by users in daily use of mobile phones. As the first remedy, a liquid silicone rubber with adhesives is fixed onto their polymer case by the liquid injection molding (LIM) process [22]. Since adhesives invoked in the silicone are responsible for joining, delamination might occur in partial after repetitive opening-and-closing operations in daily use of mobile phones. This difficulty requests us to reconsider the joining process between flexible rubber and hard plastic case in the mobile phone.

The microgrooves are formed into the stainless steel mold for injection molding [23, 24]. Silicone rubber is joined with the polycarbonate plate as a specimen for joining strength test. The measured joining strength is constant by 4 N/mm at the presence of fine microgrooves, where the thinnest silicon rubber fractures without interfacial delamination. This joinability is common to the mobile phone model. The waterproof testing demonstrates that this joined interface has sufficient integrity at high pressure state by 15 kPa.

6.1 Microgrooving into the mold for injection molding

The picosecond laser microtexturing with use of the galvanometer is employed to form the microgroove textures onto the AISI martensitic stainless steel mold. **Figure 19** depicts four microgrooved AISI420 molds with varying widths of 100, 75, 45, and 20 μm , respectively. The groove depth is constant by 10 μm . Each microgroove is shaped to have Gaussian profile irrespectively; the beam intensity profile directly reflects on this microgroove geometry. This mold is inserted into the die-set for injection molding. Polycarbonate (PC) is employed as a work material to imprint these microgroove textures onto the work surface. **Figure 20** depicts the transcribed microbump textures onto PC from the microgroove on the AISI420 mold. Both the groove width and pitch are accurately preserved through this injection molding.

6.2 Joining strength test

In the LIM process, adhesive primer is deposited onto the interface before infiltration of silicone melt in the mold-die. Since intermission between two processes is less than 2–3 s, adhesion takes place between silicon and PC-plate under the cooling stage. **Figure 21a** depicts the PC plate specimen with a silicone square ring after joining in the inside of mold-die during LIM process. In the following test, only the joined section in the width of 80 mm is used for tensile adhesive strength testing. A uniaxial

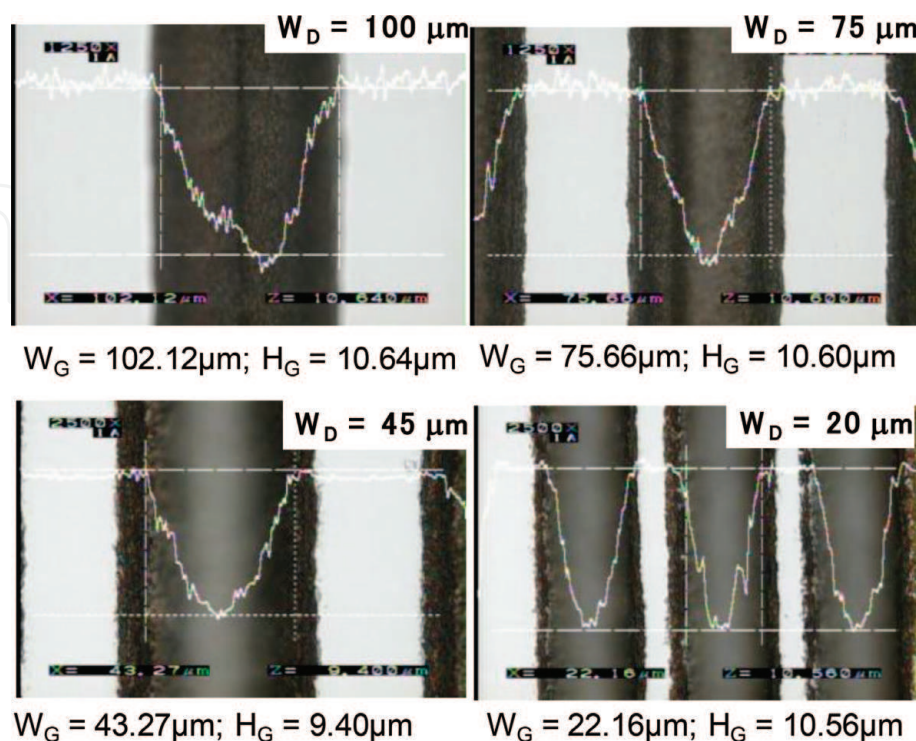


Figure 19. Microgroove textures with various widths from 100 to 20 μm and constant depth of 10 μm into AISI420 stainless steel substrate.

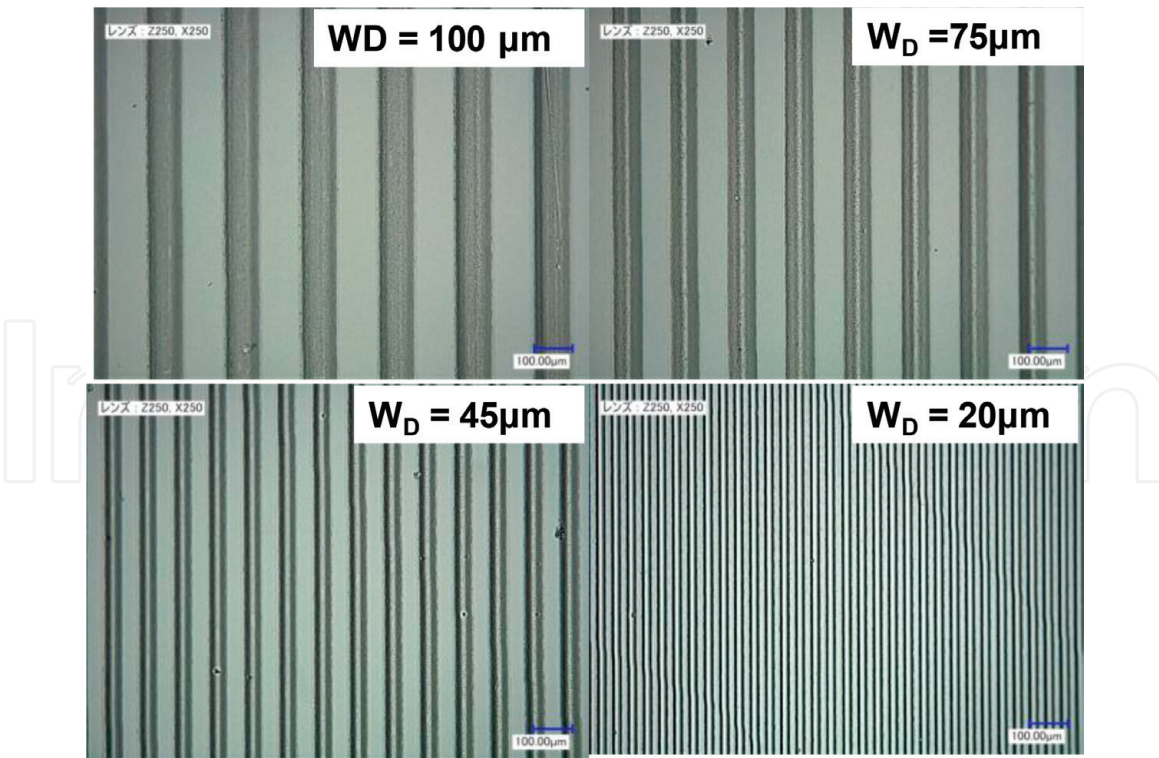


Figure 20.
Transcription from the microgrooves on the AISI420 mold to the microbumps on the PC specimen.

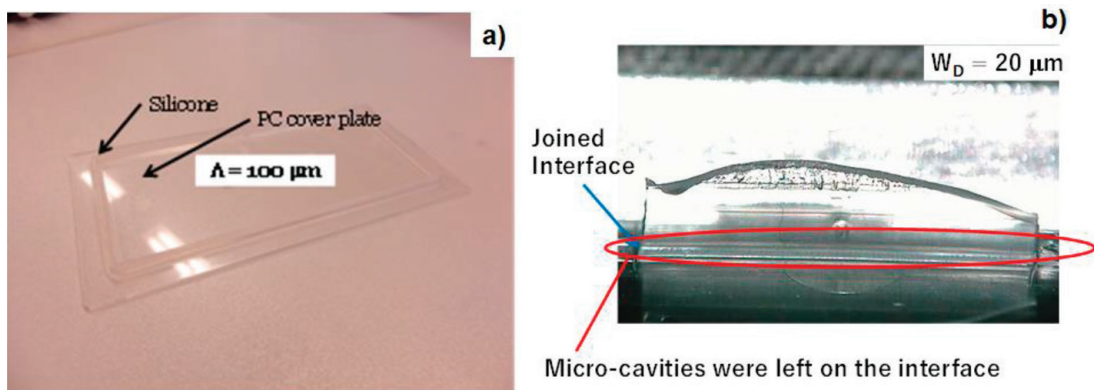


Figure 21.
Joining strength testing. (a) Microbump textured PC specimen joined with silicone rubber and (b) fatal fracture of silicone without interfacial delamination.

tensile testing system with the dynamic video monitoring is used to measure the loading behavior till the final fracture with in situ observation on the deformation of silicone. As shown in **Figure 21b**, when the microgroove width is less than the intrinsic microcavity width of $100 \mu\text{m}$, the fatal fracture occurs in the tensile silicone rubber without any delamination of interface between PC and silicone. This joining strength reaches 4 N/mm irrespective of the joined length and size even if the microcavities are present on the interface. This implies that microtextures on the joined interface could control the cavitation process to be free from interfacial delamination.

6.3 Waterproof test of cellular-phone model

The skewed microgrooves with their width and depth of $20 \mu\text{m}$ are laser-machined into the AISI420 die insert. In the similar way to preparation for the PC-specimen with the silicone rubber ring, the injection molding is used to transcribe the microgrooves into the PC-cover case; LIM process is also utilized to make

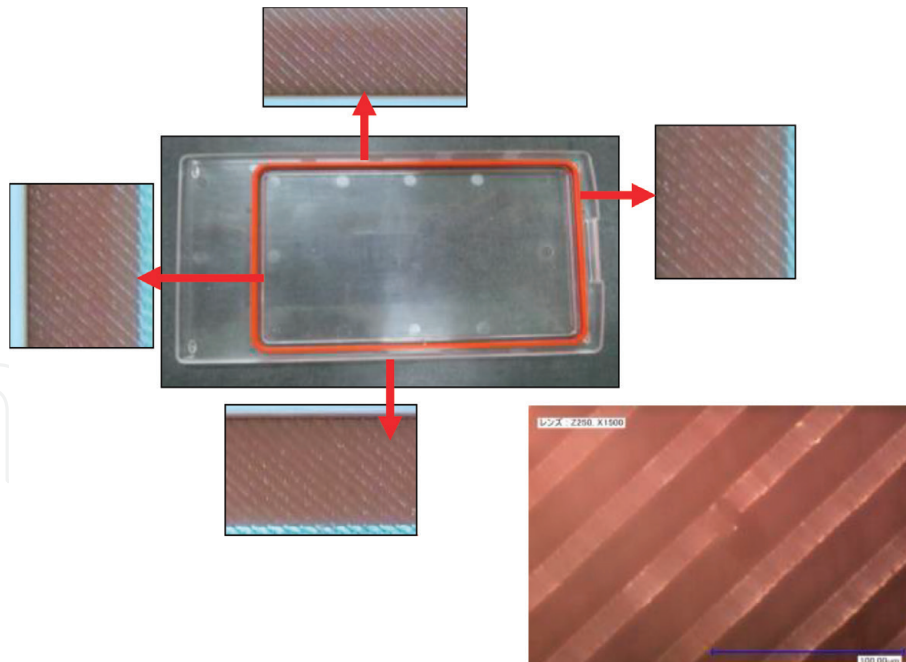


Figure 22.
 A mobile phone PC-model joined with the silicone rubber through the microtexture with the width of 20 mm on the interface.

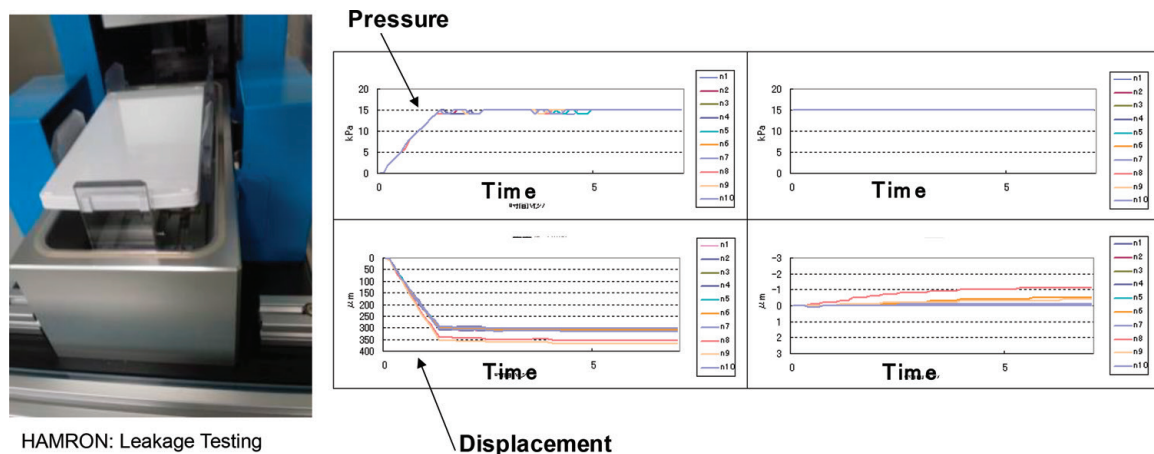


Figure 23.
 Waterproof test to demonstrate the integrity of mobile phones under the pressure of 15 kPa.

in situ joining of silicone rubber ring onto the PC-cover case via the microbump textures on PC. **Figure 22** depicts the mobile phone model, fabricated in the above procedure. Each interface between the PC-cover case and silicone rubber has microbump textures. The Hamron leakage testing is employed to perform the waterproof test; e.g., this test aims at the quality check of significant deformation by small leaks under the applied pressure for 5 min. This model is dipped into a water pool, pressurized up to 15 kPa and held for 5 min. As shown in **Figure 23**, the PC-cover case deforms by pressuring it up to 15 kPa; no further deformation is detected during the holding duration. This demonstrates the perfect waterproof on the jointed interface with aid of microbump textures.

7. Surface property control by laser nano-/microtexturing

Superhydrophilicity and superhydrophobicity have grown up as a key surface engineering to keep clean and fresh surface of products and to control the liquid

flow on the product surfaces. The oxide-glass lens as well as metallic-glass, optical elements are a typical targeting product to have their surface hydrophilic or superhydrophilic for liquid film formation, and to have it hydrophobic or superhydrophobic for well-defined water repellency [25]. The high energy surface had higher attractive capacity to other material atoms and molecules; those are adherent to each other to form a wet film on the surface. While, the low energy surface had lower attractive capacity to other material atoms and molecules; those are isolated from each other to form the droplets on the surface.

There are two modifications to control this surface state; e.g., the chemical and physical treatments. The chemical treatment is a general tool to modify the surface condition; e.g., fluorine-based coating increases the contact angle up to 130–150° in [26]. On the other hand, the idea of lotus effect has been discussed as a physical approach to form hydrophobic surface [27]. This lotus effect works in nature since the water droplets are supported by the air gap through the fine fibrous lotus leaf; this idea suggests that wettability might be widely controlled by the micro-/nanotexturing [28]. As has been reported in [29–31], the femtosecond laser micro-/nanotexturing methods have been developed to tune the surface wettability from superhydrophilic to superhydrophobic states. In particular, the micro-/submicro textures are formed on any materials by the laser-induced periodic surface structuring (LIPSS), where the incident and reflected lights have interaction with the scattered and diffracted lights at the vicinity of surface roughness [32]. Among several approaches to design this LIPSS, the authors proposed the micro-/submicrotexturing design by LIPSS with the use of fundamental wavelets and high-frequency ripples [33, 34]. Here, LIPSS is formed onto the AISI304 stainless steel substrates by using the femtosecond laser texturing. Both the superhydrophilic and superhydrophobic surfaces can be formed by the present laser nano-/microtexturing. The geometric effect of surface geometry on the superhydrophobicity is discussed to optimize the laser surface profile control.

7.1 LIPSS by femtosecond laser texturing

With reduction of the pulse duration, the optical interaction with irradiated materials localizes in the wavelength range. When irradiating the materials in the fundamental mode, this interaction field is limited within the submicrometer range. LIPSS is a typical local interaction, occurring at the site of material surface roughness in the order of micrometer. **Figure 24** depicts the LIPSS formed on the austenitic stainless steel type 304 by the present femtosecond laser texturing. Nanotexturing alignment angulates itself across the microtexture in **Figure 24a**

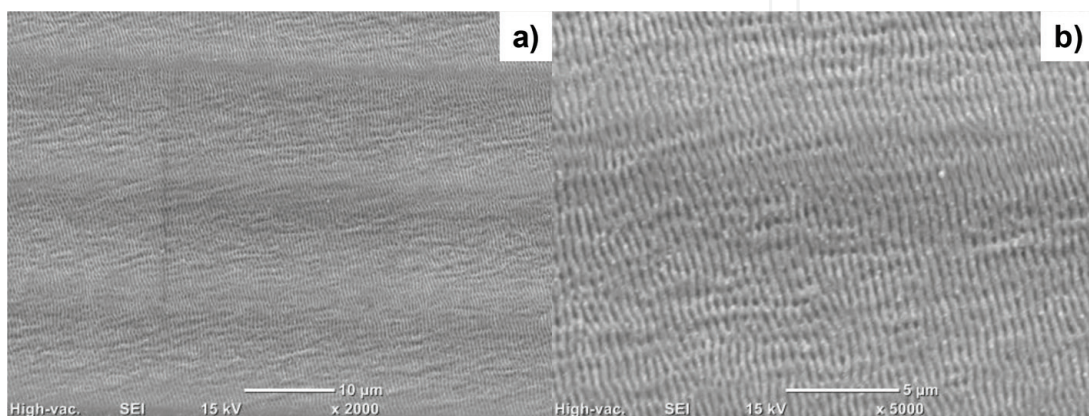


Figure 24. LIPSS formed on AISI304 substrate surface by the present femtosecond laser texturing. (a) Microtextured angulation and nanotextures and (b) fine alignment of nanotextures.

since optical interaction is affected by the surface profile in micrometer range. As shown in **Figure 24b**, the spatial periodicity of these nanotextures is constant by 250 nm. This reveals that fine nanotextures with constant periodicity are formed on the metallic surface by the femtosecond laser treatment.

7.2 Superhydrophilic surface formation

After the classical theory on the surface wettability [35], the hydrophilic or the hydrophobic surfaces are modified to have superhydrophilic or superhydrophobic states, respectively. This is because the geometric item works to decrease the contact angle for hydrophilic surface or to increase it for hydrophobic one. **Figure 25** depicts the wettability of nanotextured AISI304 surface by the femtosecond laser surface modification. The measured contact angle reaches down to 8° ; it is superhydrophilic. This reveals that the classical theory is true to describe the geometric nanotexture effect on the contact angle when the spatial periodicity of nanotextures works as a major geometric item in surface quality.

7.3 Superhydrophobic surface formation

In addition to the nanotexturing surface modification, the microtexturing angulation is taken into account as the geometric item. AISI304 stainless steel sheets with the size of $25 \times 25 \times 3 \text{ mm}^3$ are nano-/microtextured to investigate the change of surface wettability by this processing. **Figure 26** compares the droplets swelling on the specimen before and after this micro/submicrolaser texturing. The contact angle of pure water on the bare stainless steels is $70\text{--}75^\circ$, corresponding to the normal wettability of metals [36]. Through the present texturing, the contact angle

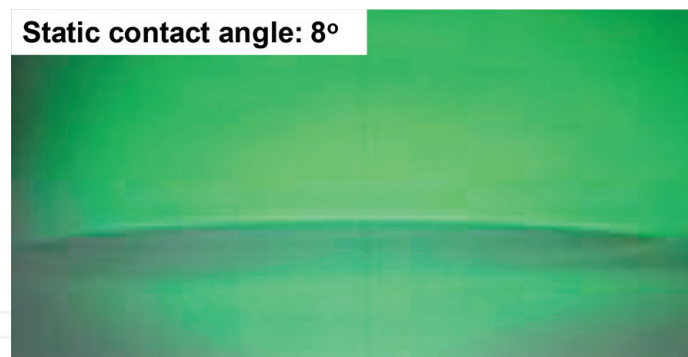


Figure 25.
Modification of hydrophilic surface to have superhydrophilic state by laser nanotexturing.

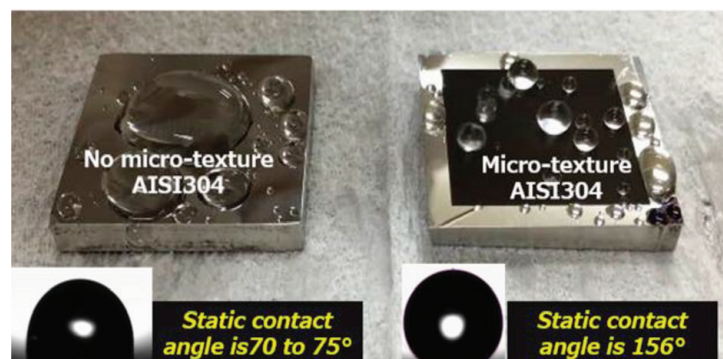


Figure 26.
Modification of wettability on the AISI304 substrate from the original hydrophilic state to the superhydrophobic one by laser nano-/microtexturing.

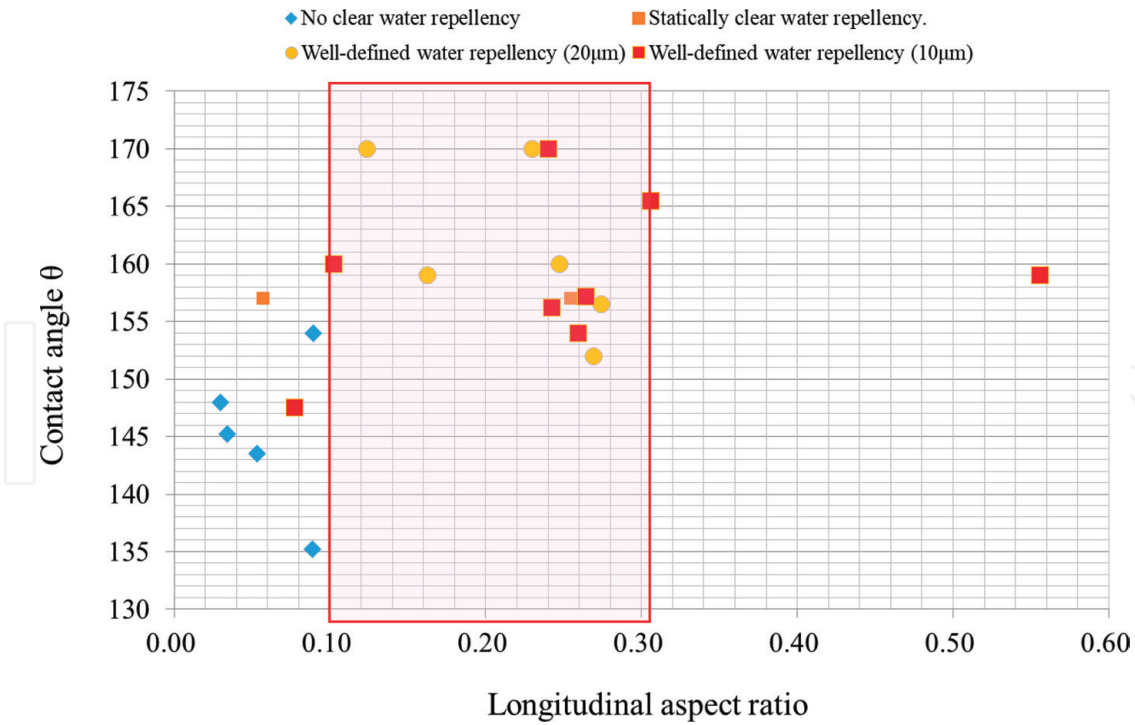


Figure 27. Effect of the longitudinal aspect ratio on the measured contact angle among 30 nano-/microtextured AISI304 substrates.

increases up to 156° . This proves that nano-/microlaser texturing provides a tool to modify the wettability of stainless steel surfaces from hydrophobic to superhydrophobic state. This finding is completely against the classical theory; if more geometric items are put into laser texturing, the material surface quality can be widely controlled by geometric design.

7.4 Optimization of surface geometric configuration

There are two geometric items affecting on the surface property; the fractal dimension and the aspect ratio for nanotextures [37]. The former influences on the complexity of surface geometry; the latter, on the local angulation of geometry. Thirty AISI304 stainless steel sheets with the size of $10 \times 10 \times 0.1$ t mm³ are laser nano-/microtextured to investigate the effect of microtexture pitch and height on the measured wettability. **Figure 27** describes the relationship between the aspect ratio of nanotexture width to height on the measured contact angle. When this aspect ratio is less than 0.1 or more than 0.3, almost all measured contact angles are less than 155° ; the micro-/submicrotextured AISI304 specimens are only hydrophobic. Higher contact angle up to 170° is attained when tuning this aspect ratio between 0.2 and 0.3; e. g., when using the microtextures with the width of 20 μm , their height might well be 2–6 μm . This implies that local angulation of surface geometry has significant influence on the controllability of hydrophobicity.

8. Friction control of tools by laser microtexturing

Under the strong demand for reduction of environmental burdens in manufacturing, every productive line must be energy-saving and highly material-efficient with less emission to environments [38]. In past, the huge amount of lubricating oils has been utilized to reduce the friction and wear not only in automobile industries but also in machining, metal forming, and so on [39]. In order to reduce this amount down to

the minimum quantity, the contact surface of mechanical parts and tool surfaces are microtextured to reduce the friction coefficient and wear rate under minimum quantity lubrication (MQL) [40]. Microdimples on the working interfaces and surfaces play as a lubricating oil pocket to form a thin lubricating oil film on the interface between sliding parts and between work materials and tools [41]. The depth profile of each microdimple reflects on the local pressure distribution; this interfacial lubricating film works as a pressure boundary to support the sufficient film thickness to lubrication under MQL [42]. In addition, these microdimples work as a reservoir to store the wear debris of work materials and tool chips during the semidry machining and metal forming [43]. Here, the microdimples are formed by the picosecond laser texturing onto the dies and tools. The pin-on-ball method is employed to evaluate on the reduction of friction for the microdimpled die. The normal milling test is also utilized to describe the effect of microdimpled cutting tool on the reduction of tool wear.

8.1 Laser microtexturing of dimples

The picosecond laser microtexturing is employed to form the circular microdimples onto the AISI420 stainless steel dies, with the diameter of 50 and 100 μm and the depth of 10 μm in the regular lattice alignment with the pitch of 100 and 200 μm , respectively, for tribotesting. While, the isosceles triangular microdimples with the bottom edge of 155 μm , the height of 80 μm and the depth of 5 μm are machined onto the WC (Co) cutting tools in the zigzag alignment. **Figure 28** depicts these microdimpled specimens and tool together with the SEM-image and three-dimensional profile of microdimples.

8.2 Tribotesting

The pin-on-ball testing is employed to measure the time evolution of frictional force under the constant normal load. In this testing, the counter material ball is on contact with the die material under the applied normal weight as depicted in **Figure 29**. The frictional force is directly measured by load sensor attached to the arm. In the following tests, SUJ2 hard balls are utilized as a counter material. The friction coefficient is calculated by division of the measured friction force to the applied normal load. **Figure 30** depicts the transients of friction coefficient with increasing

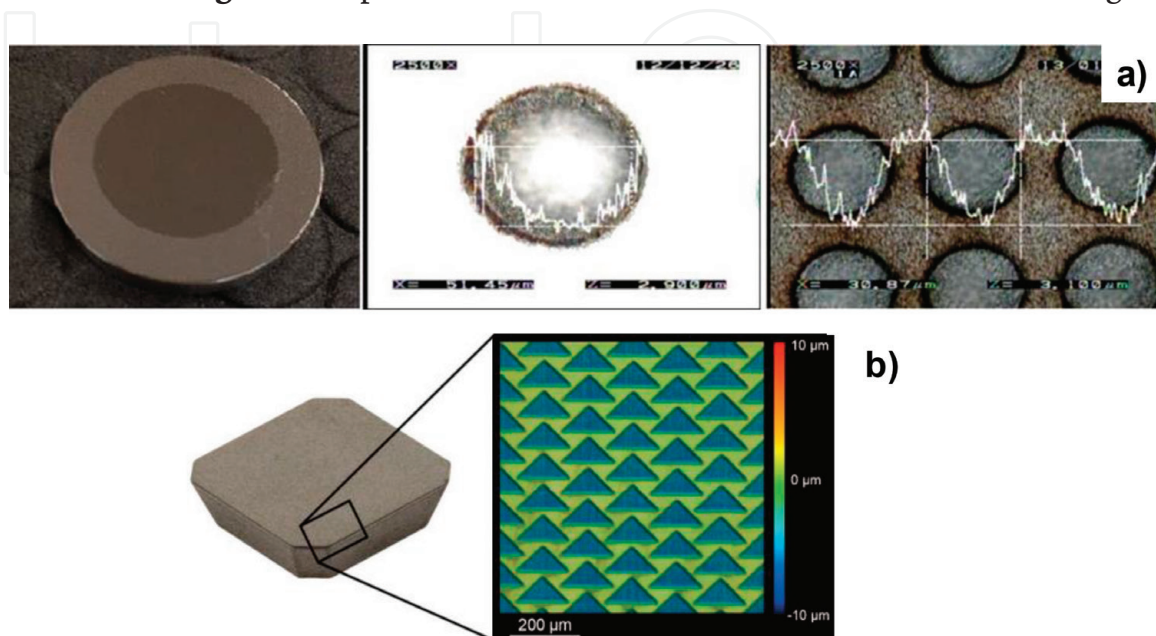


Figure 28. Laser microdimple texturing. (a) Microdimpled stainless steel die and (b) microdimpled WC (Co) cutting tool.

the sliding distance for three die specimens; e.g., a bare AISI420 die without microdimples, and two microdimpled dies with the microdimple diameter (D) of $100\ \mu\text{m}$ and its pitch (p) of $200\ \mu\text{m}$ and with $D = 50\ \mu\text{m}$ and $p = 100\ \mu\text{m}$, respectively. In case of bare die, the friction coefficient increases monotonically with sliding distance up to 0.15. When using the microdimpled die with $D = 50\ \mu\text{m}$ and $p = 100\ \mu\text{m}$, lower friction coefficient than 0.07 is preserved during this tribotesting.

8.3 Machining test

When milling the aluminum alloys by WC (Co) tools, the tool face is inevitably subjected to adhesion of work material. Microtexturing into the tool face enables to reduce this adhesion by storing the wear debris and cutting chips into these pockets on it. In this experiment, AA5052 aluminum alloy is employed as a work material for normal milling with use of the bare WC (Co) and microtextured one as shown in **Figure 28b**. **Figure 31** compares the adhesion process of work material onto the tool face at the milling distance (L) of 900 and 1800 m, respectively, between the bare and microdimpled tools. Without microdimples, the adhesive area and thickness of work materials onto the tool face enlarges with increasing L ; e.g., when

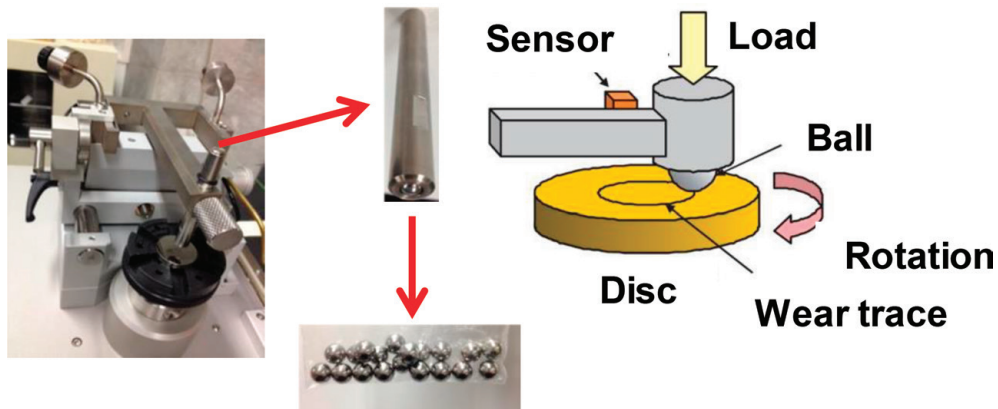


Figure 29. The ball-on-disc method for measurement of friction coefficient during the sliding conditions.

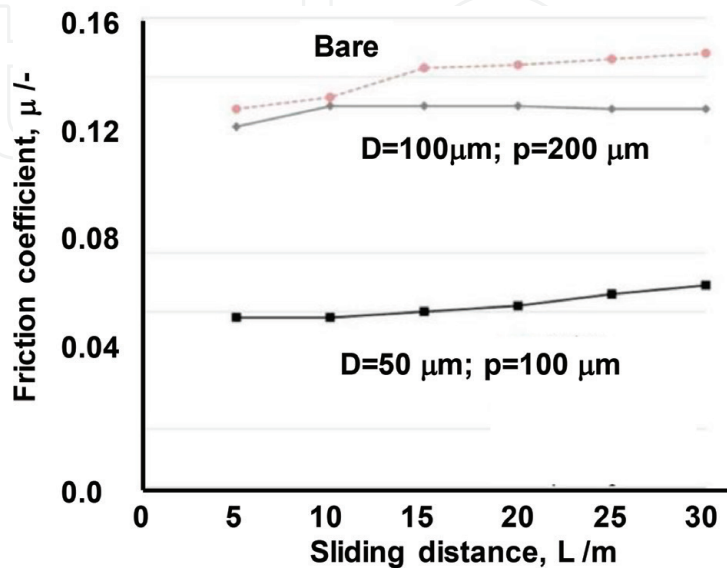


Figure 30. Variation of the friction coefficient with increasing the sliding distance for three cases; the bare die without microdimples, and the microdimpled dies with $D = 100\ \mu\text{m}$ and $p = 200\ \mu\text{m}$ and $D = 50\ \mu\text{m}$ and $p = 100\ \mu\text{m}$, respectively.

$L = 1800$ m, nearly the whole face is covered by these work adhesives with their film thickness of $10\ \mu\text{m}$ around the tool edge. On the other hand, little adhesion to microdimpled face is noted even after milling up to 1800 m. This significant reduction of adhesion by microtexturing comes from the storing mechanism where the wear debris and cutting chips are reserved into each microdimple. This reduction of adhesion influences on the cutting force; e.g., the cutting force becomes relatively insensitive to cutting distance when using these microtextured tools.

8.4 Applications

Low friction and wear is indispensable for most of automotive parts and manufacturing tools. They have curved surfaces, the friction coefficient of which must be reduced to save the energy waste and to improve the fuel efficiency. In particular,

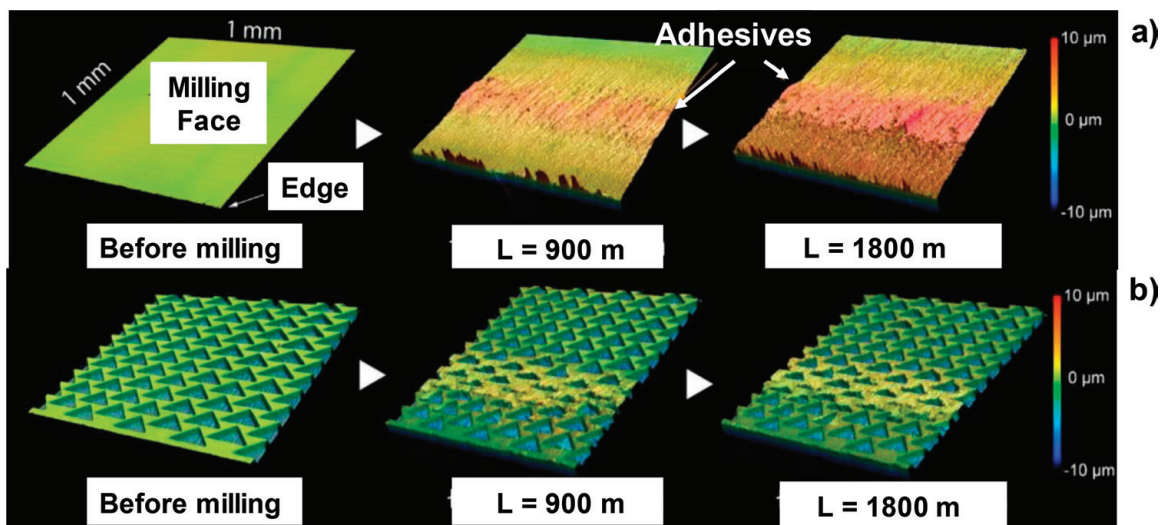


Figure 31.
 Comparison of work material adhesion to tool face with increasing the milling distance between the bare and microdimpled WC (Co) tools.

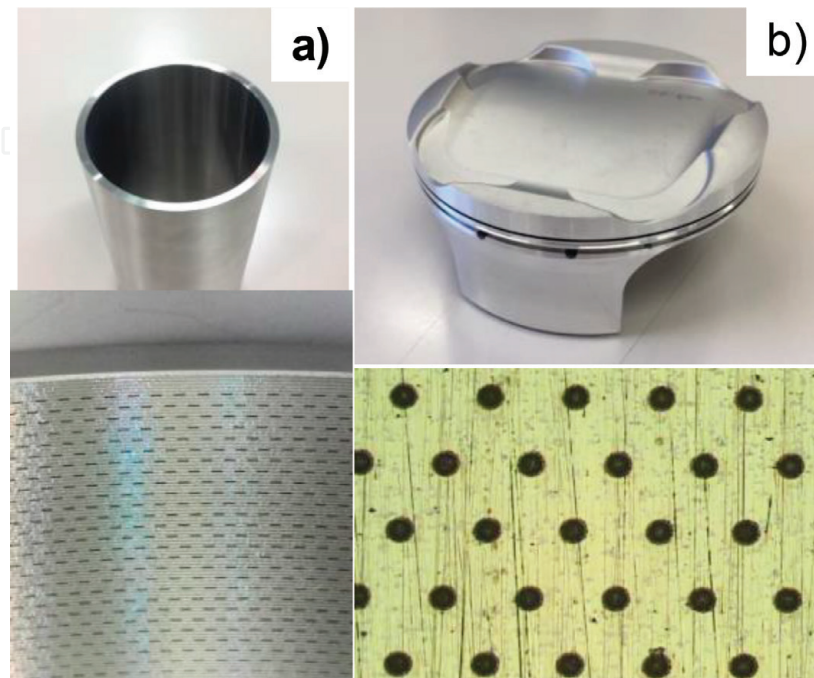


Figure 32.
 Microtexturing into the inner surfaces of automotive parts. (a) Microtextured piston cylinder and (b) microtextured piston skirt.

the piston cylinder as well as piston skirt are important sliding-part. **Figure 32a** shows the microdimpled AISI316L inner surface of cylinder with the size of $30 \times 500 \mu\text{m}^2$ and the depth of $5 \mu\text{m}$ in the pitch of 1 mm in the circumferential direction and 0.5 mm along the length. This wedge-shaped microdimples improve the fuel efficiency significantly. The AA7075 piston skirt is also microdimpled to have circular dimples with the diameter of $30 \mu\text{m}$, the depth of $3 \mu\text{m}$ and the pitch of $120 \mu\text{m}$, respectively, as shown in **Figure 32b**.

9. Discussion

The spatial resolution in this laser machining is first discussed to find out the way to improve its dimensional accuracy. Through the practical survey on the micromachining and texturing into curved surfaces, the feasible applications are understood to search for bio-medical laser processing. In particular, future trend of fast-rate laser technologies is discussed for further improvement of micromachining.

9.1 Spatial resolution in laser micromachining

Laser drilling of circular holes is employed as a benchmark test to discuss the dimensional accuracy of 25×25 holes in square structure with the diameter of $30 \mu\text{m}$ and the pitch of $50 \mu\text{m}$, as depicted in **Figure 33a**. Silicon nitride plate with the thickness of $125 \mu\text{m}$ is used as a work material. **Figure 33b** and **c** shows the

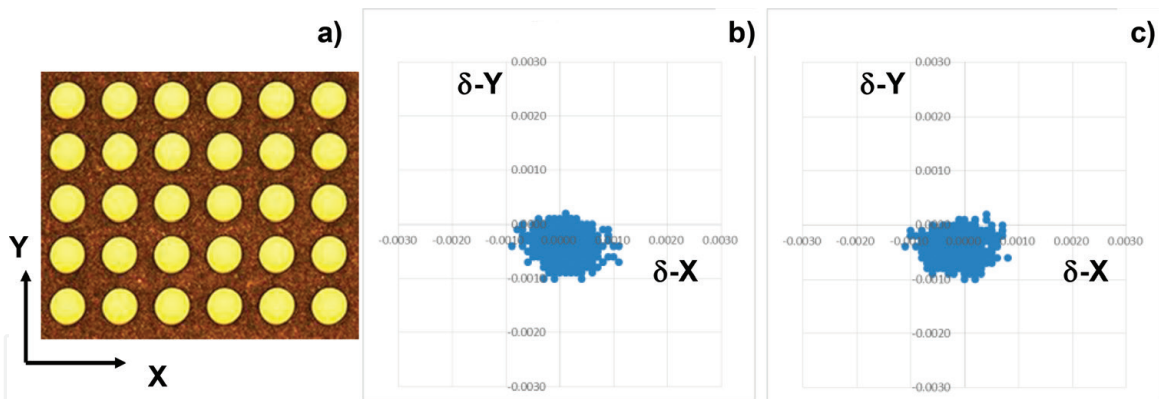


Figure 33. Benchmark test to investigate the dimensional accuracy in the laser microdrilling. (a) Test-drilling, (b) deviation map, measured at the inlet, and (c) deviation map, measured at the outlet.

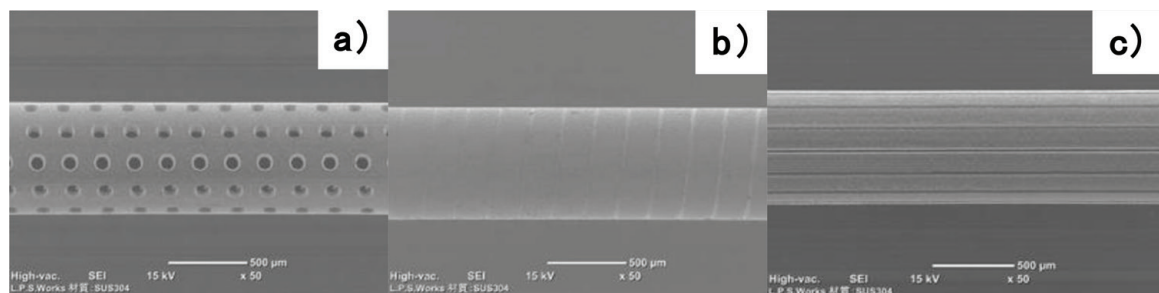


Figure 34. Microtexturing into the metallic tube. (a) Microdrilling of holes with the diameter of $100 \mu\text{m}$ into a AISI304 stainless steel pipe with $D_{\text{out}} = 0.7 \text{ mm}$ and $D_{\text{in}} = 0.58 \text{ mm}$, (b) microgrooving of shallow grooves with the width of $25 \mu\text{m}$ and the depth of $3 \mu\text{m}$ into the same pipe as (a), and (c) microgrooving of lateral grooves with the depth of $30 \mu\text{m}$ into the same pipe as (a).

X- and Y-deviation maps at the inlet diameter and outlet diameter for 625 holes. Since both maps are nearly coincident to each other, the straightness and circularity are preserved to be within $1/125 \mu\text{m} \sim 0.7^\circ$, and within $2 \mu\text{m}$, respectively. The spatial resolution of hole diameter is within $2.5 \mu\text{m}$ in the 2σ -reliability.

9.2 Laser micromachining into curved surfaces

Without specially designed jigs and fixtures, both the micromilling and micro-EDM are difficult or nearly impossible to microdrill the holes and grooves. Laser microdrilling has little constraint in the manufacturing setup; it is readily applied to make direct drilling. AISI304 stainless steel pipe with its outer diameter (D_{out}) of 0.7 mm and its inner diameter (D_{in}) of 0.58 mm is employed as a work to make microdrilling the holes and grooves. **Figure 34** shows three microtexturing cases; e.g., a microdrilled pipe, a spiral-grooved pipe, and a laterally grooved pipe. The designed textures can be accommodated to the curved surfaces by this laser microdrilling.

Another feature of laser microtexturing is developed by changing the beam control. A thin spring is structured from a pipe in **Figure 35a**. A wide slit is structured into a pipe as depicted in **Figure 35b**. Any shaped short-cuts are equipped into a pipe as shown in **Figure 35c**. This suggests that complex microstructure can be built in the micromachine and micromember.

9.3 Laser micropart formation from pipes

Let us discuss how to make laser-structuring a micropart from commercial components. A polylactic acid (PLA) pipe is employed as a starting component to fabricate the PLA-stents for medical usage. **Figure 35** depicts three PLA-stents fabricated from the same PLA-pipe by the laser microtexturing. These three can be selectively made from PLA-pipe only by varying the slit width (Ws) to be 154 ,

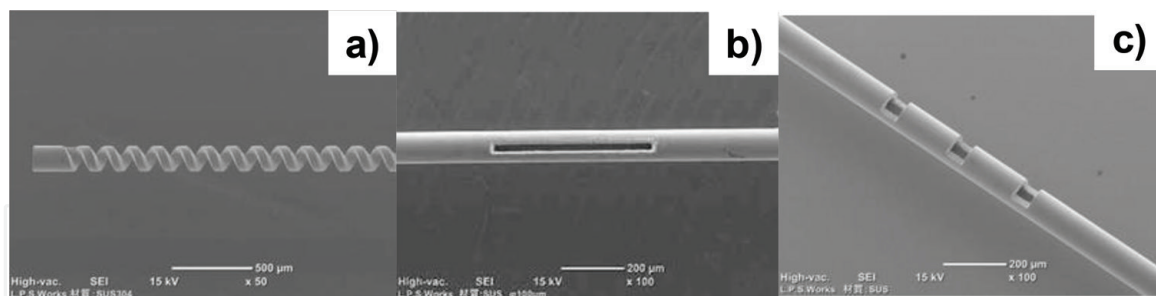


Figure 35. Fabrication of the geometrically functionalized parts by laser microtexturing. (a) Structuring a spring with the pitch of $150 \mu\text{m}$ from thin brass pipe with $D_{\text{out}} = 160 \mu\text{m}$ and $D_{\text{in}} = 80 \mu\text{m}$, (b) structuring a slit with the size of $30 \times 500 \mu\text{m}^2$ into AISI304 stainless steel pipe with $D_{\text{out}} = 100 \mu\text{m}$, and (c) fabrication of short-cuts with the size of $65 \times 50 \mu\text{m}^2$ from the same pipe as (b).

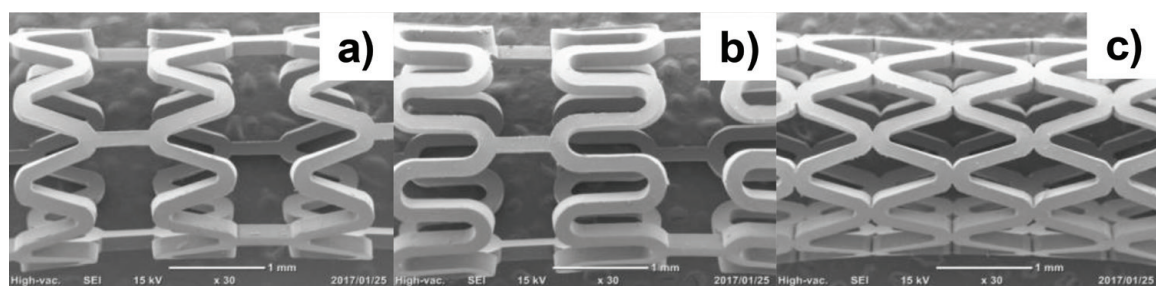


Figure 36. Laser micropart formation of stents from PLA pipe with $D_{\text{out}} = 2.55 \text{ mm}$, $D_{\text{in}} = 2.20 \text{ mm}$, and the length of 25 m . (a) $Ws = 154 \mu\text{m}$, (b) $Ws = 156 \mu\text{m}$, and (c) $Ws = 160 \mu\text{m}$.

156 and 160 micro-meter, respectively. The topological geometry of stents can be designed and fabricated for each medical treatment by tuning the laser microtexturing parameters as shown in **Figure 36**.

9.4 Future trends in laser micromanufacturing

Various geometric transformations can be realized only by the laser processing such as the micromachining, microtexturing, and microstructuring in the above. Through the fusion of other manufacturing treatments with the laser processing, further advancement is expected to propose the innovative procedures. With combination of laser nano-/microtexturing with laser polishing, the surface property is selectively controlled to be superhydrophilic or superhydrophobic by tuning the LIPSS-conditions. With combination of laser microtexturing with the mechanical milling, a multimaterial part as well as a structural member with large area can be functionalized as a complex-shaped part or as a functionalized component.

Among the engineering issues related to ultrashort pulse laser processing, how to put the fast-rate microtexturing into practice is one of the important targets. In addition to increase of repetition frequency in laser oscillation, new optical control must be developed to transform the spatial geometry and topology in shape into time sequence of scanning in beam technology.

10. Conclusion

The picosecond and femtosecond laser processing is designed to be tools for advanced manufacturing; laser microdrilling, laser microtexturing, laser nano-/microtexturing, laser microstructuring, and so on. The dimensional accuracy, the spatial resolution as well as the circularity approaches to 1 μm or less than; every micropart, every microstructure, and every microtexture is fabricated in the product size of 10 to 100 μm range. Most of engineering issues related to surface and interface are well defined in this laser processing to find an optimum solution to each problem. Reduction of friction and wear in tools and works is attained by microtexturing onto the tool and part surfaces. Reliable joining between dissimilar materials and parts is put into practice by chemical adhesion with aid of microtextures on their interface. Surface and interface properties are also controllable by optimization of nano-/microtextures.

Sustainable manufacturing requires for the well-designed processing to support the efficient circulation of products, parts, and materials in addition to recycle and reuse of second hands. Laser micromachining is useful to prolong the tool life, to revise the product surfaces and interfaces for multiple use and to assist the multi-materialization for second-hand products and parts.

Further research and development on the unknown features of laser processing is necessary to advance new steps in innovative technology and medical engineering to further improve the sustainability in future society.

Acknowledgements

The authors would like to express their gratitude to Mr. T. Hasegawa, T. Miyagawa (SIT), Dr. K. Wasa (TecDia, Co. Ltd.), Mr. T. Omata, and Mr. K. Sanbongi (LPS-works, Co. Ltd.) for their help in experiments. The present study was financially support in part by the METI with Supporting-Industry Projects in Japanese Government from 2010 to 2017.

Conflict of interest

The authors declared no conflict of interest.

IntechOpen

Author details

Tatsuhiko Aizawa^{1*} and Tadahiko Inohara²

1 Surface Engineering Design Laboratory, Shibaura Institute of Technology, Tokyo, Japan

2 LPS Works, Co. Ltd., Tokyo, Japan

*Address all correspondence to: taizawa@sic.shibaura-it.ac.jp

IntechOpen

© 2019 The Author(s). Licensee IntechOpen. This chapter is distributed under the terms of the Creative Commons Attribution License (<http://creativecommons.org/licenses/by/3.0>), which permits unrestricted use, distribution, and reproduction in any medium, provided the original work is properly cited. 

References

- [1] Avanish D. Laser beam machining—A review. *International Journal of Machine Tools and Manufacture*. 2008;**48**:609-628
- [2] Davim P. *Nontraditional Machining Processes: Research Advances*. New York: Springer; 2013
- [3] Schmid K. *Manufacturing Processes for Engineering Materials*. 5th ed. New Jersey: Prentice Hall; 2008
- [4] Aizawa T, Iohara T. Japan Patent. 2011-212046; 2011
- [5] Gaertner E, Polise V, Tagliaferri F, Palumbo B. Laser micro machining of alumina by a picosecond laser. *Journal of Laser Micro/Nanoengineering*. 2018;**13**:76-84
- [6] Amer MS, Ei-Ashry MA, Dosser LR, Hix KE, Maguire JF, Irwin B. Femtosecond versus nanosecond laser machining: Comparison of induced stresses and structural changes in silicon wafers. *Applied Surface Science*. 2005;**242**:162-167
- [7] Nasrollahi V, Penchev P, Dimov SS. A new laser drilling method for producing high aspect ratio micro holes. In: *Proc. 11th 4M Conf.* 2016. pp. 15-18
- [8] Aizawa T, Inohara T. Micro-texturing onto glassy carbon substrates by multi-axially controlled pico-second laser machining. In: *Proc. 7th ICOMM*. 2012. pp. 66-73
- [9] Aizawa T, Inohara T. Multi-dimensional micro-patterning onto ceramics by pico-second laser machining. *Research Reports of Shibaura Institute of Technology. Natural Sciences and Engineering*. 2012;**56**(1):17-26
- [10] Tokura K. Machining process. Japanese textbook for mechanical engineering. The Japan Society of Mechanical Engineers. 2006;**5**:111
- [11] Doering S, Richter S, Molte S, Tuennemann A. In-situ observation of the hole formation during deep drilling with ultra-short pulses. *Proceedings of SPIE*. 2011;**7925**:792517:1-792517:8
- [12] Doering S, Richter S, Nolte S, Tuennemann A. In-situ imaging of hole shape evolution in ultra-short pulse drilling. *Optics Express*. 2010;**18**:20395-20400
- [13] Ashkenasi D, Mueller N, Kaszemeikat T, Illing G. Advanced laser micro machining using a novel trepanning system. *Journal of Laser Micro/Nanoengineering*. 2011;**6**(1):1-5
- [14] Aizawa T, Inohara T. Pico-second laser drilling of high-aspect ratio through-holes with and without tapering. In: *Proc. 1st WCMNM*. Vol. 103. 2017. pp. 1-2
- [15] Aizawa T, Wasa K, Tamagaki H. A DLC-punch array to fabricate the micro-textured aluminum sheet for boiling heat transfer control. *Micromachines*. 2018;**9**:147-1-147-10
- [16] Denkena B, Koehler J, Kaestner J. Efficient machining of micro-dimples for friction reduction. In: *Proc. 7th ICOMM*. 2012. pp. 85-89
- [17] Jiang Y, Zhao WS, Kang XM, Gu L. Adaptive control for micro-hole EDM process with wavelet transform detecting method. In: *Proc. 6th ICOMM*. 2011. pp. 207-211
- [18] Aizawa T, Fukuda T. Oxygen plasma etching of diamond-like carbon coated mold-die for micro-texturing. *Surface and Coating Technology*. 2013;**215**:364-368

- [19] Aizawa T, Itoh K, Inohara T. Imprinting of patterns onto polymers and oxide-glasses via fine micro-stamping. In: Proc. 6th ICOMM. 2010. pp. 77-82
- [20] Aizawa T. Micro-texturing onto amorphous carbon materials as a mold-die for micro-forming. *Applied Mechanics and Materials*. 2013;**289**:23-37
- [21] Balden A. Adhesively bonded joints and repairs in metallic alloy, polymers and composite materials: Adhesives, adhesion theories and surface pretreatment. *Journal of Materials Science*. 2004;**39**:1-49
- [22] Available from: <http://www.shinetsu.co.jp/> [Accessed: Nov 30, 2018]
- [23] Aizawa T, Satoh S, Yamaguchi T. Micro-texturing design for joining between polymer components. In: Proc. 9th ICOMM. Vol. 15. 2014. pp. 1-8
- [24] Aizawa T, Satoh S, Yamaguchi T. Joining of polymer systems by micro-texturing toward perfect water-proof. *Research Report, SIT*. 2014;**58**:1-10
- [25] Packham DE. Surface energy, surface topography and adhesion. *International Journal of Adhesion and Adhesives*. 2003;**23**:437-448
- [26] Nakamae K. How to form the hydrophobic and super-hydrophobic surfaces in industries. *Industrial Materials*. 1996;**44**:26-30
- [27] Cheng YT, Rodak DE. Is the lotus leaf superhydrophobic? *Applied Physics Letters*. 2005;**86**:144101
- [28] Aizawa T. Micro-texturing for tribology and surface engineering in manufacturing processes. In: *Proceedings ISAST IV*. 2016. pp. 1-16
- [29] Hoehm S, Rosenfeld A, Krueger J, Bonse J. Femtosecond laser-induced periodic surface structures on silica. *Journal of Applied Physics*. 2012;**112**:0149010-0149019
- [30] Orazi L, Gnilitzky I, Serro AP. Laser nanopatterning for wettability applications. *Journal of Micro and Nano-Manufacturing*. 2017;**5**:0210081-0210088
- [31] Kietziga AM, Mirvakilia MN, Kamalb S, Englezosa P, Hatzikiriakos SG. Laser-patterned super-hydrophobic pure metallic substrates: Cassie to wenzel wetting transitions. *Journal of Adhesion Science and Technology*. 2011;**25**:2789-2809
- [32] Gečys P, Vinčiūnas A, Gedvilas M, Kasparaitis A, Lazdinas R, Račiukaitis G. Ripple formation by femtosecond laser pulses for enhanced absorptance of stainless steel. *Journal of Laser Micro/Nanoengineering*. 2015;**10**:129-133
- [33] Hasegawa T, Aizawa T, Inohara T, Wasa K. Fabrication and control of super-hydrophobic surfaces by the femto-second laser machining. In: Proc. 1st World Congress on Micro and Nano Manufacturing. 2017. pp. 381-382
- [34] Hasegawa T, Aizawa T, Inohara T, Wasa K. Engineering design for super-hydrophobic surfaces via the femto-second laser machining. In: Proc. 10th Asian Workshop on Micro/Nano Forming Technology. 2017. pp. 33-34
- [35] Kawase T. Super-hydrophobic surface. In: *SEM'I GAKKAI*. Vol. 65. 2009. pp. 200-207
- [36] Kam DH, Bhattacharya S, Mazumder J. Control of the wetting properties of an AISI 316L stainless steel surface by femtosecond laser induced surface modification. *Journal of Micromechanics and Microengineering*. 2012;**22**:1-6
- [37] Hasegawa T, Aizawa T, Inohara T, Wasa K. Hot mold stamping of optical

plastics and glasses with transcription of super-hydrophobic surfaces. *Procedia Manufacturing*. 2018;**13**:1437-1444

[38] Allwood JM, Cullen JM. *Sustainable Materials*. Cambridge: UIT; 2012

[39] Kataoka S. Influence of lubricants on global environment. *Journal of the Japan Society for Technology of Plasticity*. 2005;**46**:4-10

[40] Czichos H, Habig K-H. *Tribologie-Handbuch (Tribology handbook)*. 2nd ed. Wiesbaden: Vieweg Verlag; 2003

[41] Aizawa T, Morita H. Dry progressive stamping of copper-alloy snaps by the plasma nitrided punches. *Materials Science Forum*. 2018;**920**:28-33

[42] Aizawa T, Morita H. Tribological design and engineering in surface treatment for semi-dry and dry stamping. In: *Proc. ICTMP*. 2016. pp. 14-28

[43] Sugihara T, Enomoto T. Performance of cutting tools with dimple textured surfaces: Comparative study of different texture patterns. *Journal of the International Societies for Precision Engineering and Nanotechnology*. 2017;**49**:52-60